

NACA RM No. L9B23a

~~115.4~~
~~NH-25-1/4~~
c.2



RESEARCH MEMORANDUM

MEASUREMENTS OF AERODYNAMIC CHARACTERISTICS OF
A 35° SWEEPBACK NACA 65-009 AIRFOIL MODEL
WITH $\frac{1}{4}$ -CHORD HORN-BALANCED FLAP BY
THE NACA WING-FLOW METHOD

By

Harold I. Johnson and B. Porter Brown

Langley Aeronautical Laboratory
Langley Air Force Base, Va.

CLASSIFICATION CANCELLED

CLASSIFIED DOCUMENT

This document contains classified information affecting the National Defense of the United States within the meaning of the Espionage Act, USC 50:31 and 32. Its transmission or the revelation of its contents in any manner to an unauthorized person is prohibited by law. Information so classified may be imparted only to persons in the military and naval services of the United States and to civilian officers and employees of the Federal Government who have a legitimate interest therein, and to United States citizens of known loyalty and discretion who of necessity are so informed thereof.

~~CONFIDENTIAL~~ NACA R 7 2420 Date 8/18/54
See 8/31/54

NATIONAL ADVISORY COMMITTEE FOR AERONAUTICS

WASHINGTON

April 18, 1949



NATIONAL ADVISORY COMMITTEE FOR AERONAUTICS

RESEARCH MEMORANDUM

MEASUREMENTS OF AERODYNAMIC CHARACTERISTICS OF

A 35° SWEEPBACK NACA 65-009 AIRFOIL MODEL

WITH $\frac{1}{4}$ -CHORD HORN-BALANCED FLAP BY

THE NACA WING-FLOW METHOD

By Harold I. Johnson and B. Porter Brown

SUMMARY

This investigation is the second of a series concerned with the determination of the fundamental characteristics of trailing-edge controls at transonic speeds. A typical sweptback airfoil model of low aspect ratio ($A = 3.04$) and zero taper which represents either a wing or a tail surface is being fitted with various $\frac{1}{4}$ -chord full-span flaps differing only in type of aerodynamic balance. The first series of tests were run with a plain flap, that is, a flap representing the case of zero aerodynamic balance. Results from those tests have been reported previously. The present tests were made with a flap that incorporated a relatively large horn balance. Some of the important results from these tests are summarized below.

The lift characteristics of the horn-balanced-flap model were similar to those of the plain-flap model; however, the lift-curve slope was, on an average, 12 percent less throughout the Mach number range tested ($M = 0.55$ to 1.15) and the flap effectiveness was somewhat lower at subsonic speeds. The horn balance eliminated approximately three-quarters of the unbalanced hinge moment due to deflection below a Mach number of 0.90. In this speed range the horn-balanced flap had a strong positive floating tendency. The horn balance did not, however, show promise as an effective aerodynamic balance at supersonic speeds because at $M = 1.05$, the hinge moments due to deflection were only 13 percent less than those measured on an equivalent unbalanced flap.

INTRODUCTION

A typical sweptback airfoil-flap combination which represents either a wing or tail surface is being tested with various $\frac{1}{4}$ -chord full-span flaps differing only in type of aerodynamic balance. Although the lift and pitching moments of the model with flap fixed are being measured also,

the primary objectives of this investigation are to study flap effectiveness and methods of balancing control surfaces at transonic speeds. The characteristics of a plain flap have been determined and were reported in reference 1. The present investigation, the second of a series, covers tests of a flap having a horn balance that was designed to give a high degree of aerodynamic balance at low speeds.

The tests consisted of measurements of the lift, pitching moments, and hinge moments acting on a semispan airfoil-flap model having a sweepback angle of 35° , an aspect ratio of 3.04, a taper ratio of 1.0, an NACA 65-009 airfoil section in planes perpendicular to the leading edge, and a full-span, $\frac{1}{4}$ -chord horn-balanced flap with unsealed gap. Forces and moments were measured over an angle-of-attack range from -5° to 15° for flap settings of 0° and 5° and for a flap deflection range from about -25° to 20° for angle-of-attack settings of 0° and 5° . Data were obtained for Mach numbers from 0.55 to 1.15 and for Reynolds numbers from about 500,000 to 1,400,000. Inasmuch as the tests were run within two widely separated altitude ranges, it was possible to ascertain some effects of Reynolds number even though the highest Reynolds number encountered was still relatively very small in comparison with anticipated full-scale Reynolds numbers.

SYMBOLS

M	average Mach number over model
M_A	airplane free-stream Mach number
R	Reynolds number
q_A	airplane free-stream dynamic pressure
q	average dynamic pressure over model
C_{L_A}	airplane lift coefficient $\left(\frac{\text{Airplane lift}}{q_A S_A} \right)$
C_L	model lift coefficient $\left(\frac{\text{Model lift}}{qS} \right)$
C_m	model pitching-moment coefficient (measured about axis 18.7 percent M.A.C. ahead of leading edge of M.A.C.) $\left(\frac{\text{Model pitching moment}}{qb\bar{c}^2} \right)$

- C_h model hinge-moment coefficient $\left(\frac{\text{Model hinge moment}}{q b_f \bar{c}_f^2} \right)$
- $C_{L\alpha}$ variation of model lift coefficient with angle of attack,
per degree $\left(\frac{\partial C_L}{\partial \alpha} \right)$
- $C_{L\delta}$ variation of model lift coefficient with flap deflection,
per degree $\left(\frac{\partial C_L}{\partial \delta_f} \right)$
- $C_{m\alpha}$ variation of model pitching-moment coefficient with angle of
attack, per degree $\left(\frac{\partial C_m}{\partial \alpha} \right)$
- $C_{m\delta}$ variation of model pitching-moment coefficient with flap
deflection, per degree $\left(\frac{\partial C_m}{\partial \delta_f} \right)$
- a.c. aerodynamic center
- c.p. center of pressure of load caused by flap deflection
- $C_{h\alpha}$ variation of flap hinge-moment coefficient with model angle of
attack, per degree $\left(\frac{\partial C_h}{\partial \alpha} \right)$
- $C_{h\delta}$ variation of flap hinge-moment coefficient with flap deflection,
per degree $\left(\frac{\partial C_h}{\partial \delta_f} \right)$
- $\frac{\partial \alpha}{\partial \delta}$ flap relative effectiveness $\left(\frac{\partial C_L / \partial \delta_f}{\partial C_L / \partial \alpha} \right)$
- α angle of attack; angle between model chord plane and direction
of relative wind
- δ_f or δ flap deflection; angle between flap chord line and airfoil
chord line measured in plane perpendicular to hinge line
- Λ sweepback angle
- λ taper ratio

A	aspect ratio
b	model span normal to wind direction (corresponds to semispan of a complete wing)
c	model chord parallel to wind direction
\bar{c}	model mean aerodynamic chord (M.A.C.)
S	total area of model (corresponds to one-half the area of a complete wing)
b_f	flap span along hinge line (corresponds to one-half the span of a full-span flap on a complete wing)
\bar{c}_f	flap root-mean-square chord perpendicular to the hinge line
c_f	flap chord parallel to wind direction
S_f	flap area rear of hinge line
\bar{c}_H	horn root-mean-square-chord perpendicular to hinge line
S_H	horn area forward of hinge line
B	horn balance coefficient $\left(\sqrt{\frac{S_H \bar{c}_H}{S_f \bar{c}_f}} \right)$
S_A	airplane wing area
ϕ	included trailing-edge angle of flap

APPARATUS

In general the recording equipment was the same as that described in reference 1. The model was mounted on the upper surface of the right wing of an F-51D airplane as shown in figure 1. Some typical variations of local velocity near the wing surface in a fore and aft direction through the model location are shown in figure 2. The diminution of velocity with increasing vertical distance from the F-51D wing surface is shown in figure 3. Model force and moment coefficients were calculated by using an average dynamic pressure corresponding to the average Mach number over the model area, taking into account both the chordwise and spanwise variations of local Mach number over the model. As indicated by figure 3, no allowance was made for the wing boundary layer in calculating the average Mach number over the model; however, measurements on other F-51 airplanes indicate that the total thickness of the boundary layer at

the model test location is only about $\frac{1}{4}$ -inch so that the effect of the boundary layer on the velocity distribution over the model is believed to have been negligible. The effects of model flexibility were small and therefore considered negligible. These effects are discussed more thoroughly in reference 1.

A drawing of the horn-balanced model, including a list of pertinent dimensions is given in figure 4. The model was solid dural and a thin circular end-plane was attached at the root, of diameter equal to the model chord. The gap at the flap leading edge which amounted to about $\frac{1}{2}$ -percent airfoil chord was not sealed. The inboard edge of the horn had relatively sharp corners (chamfer approx. 0.01 in.) which were presented obliquely to the air stream in any flap-deflected condition.

The lift, pitching moment, and hinge moment acting on the model were measured by a strain-gage balance and recorded continuously by a recording galvanometer. Since the tests of reference 1, a variable angle-of-attack mechanism was added to the balance so that flights could be made with the entire model oscillating through an angle-of-attack range with fixed flap deflection as well as with the flap oscillating through a deflection range with a fixed angle-of-attack setting of the model. The position of the model with respect to the longitudinal axis of the F-51D airplane and the position of the flap with respect to the chord line of the model were measured by slide-wire potentiometers and recorded continuously by the same galvanometer that recorded the forces and moments acting on the model. All the foregoing records were synchronized by a $\frac{1}{100}$ -second timer.

The angle of flow at the model test station was measured by a calibrated freely floating vane located $22\frac{1}{2}$ inches outboard from the model test station. (See fig. 1.)

Standard NACA recording instruments were used to measure the airspeed, altitude, normal acceleration, and lateral acceleration of the airplane and the free-air temperature. These quantities were synchronized with the model records by a $\frac{1}{10}$ -second timer common to all the instruments.

TESTS

The data presented herein were obtained largely from four flights. In two of these flights the flap was fixed at deflections of 0° and 5° successively and the entire model was oscillated through an angle-of-attack range of -5° to 15° . In the other two flights the angle of attack was fixed

at 0° and 5° successively and the flap was oscillated through a deflection range of approximately -25° to 20° . In all cases the rate of oscillation was slightly greater than one cycle per second; this rate of oscillation was found to be very satisfactory because it allowed the acquisition of data throughout the entire angular ranges at approximately constant Mach number without introducing any difficulty ascribable to aerodynamic lag.

Each flight was made up of two test runs referred to hereinafter as the "high-dive" run and the "level-flight" run. The high-dive run was made by diving the airplane from 28,000 feet and an indicated airspeed of 220 miles per hour to an airplane Mach number of 0.73 at approximately 18,000 feet. During this run usable data were obtained for average Mach numbers over the model ranging from 0.65 to 1.15 at relatively lower Reynolds numbers. The level flight run was made by gradually slowing the airplane from 450 miles per hour to 300 miles per hour at 5,000 feet altitude following a dive and pull-out from about 15,000 feet altitude. During this run usable data were obtained for average Mach numbers over the model ranging from 0.55 to 0.95 (sometimes 1.0) at relatively higher Reynolds numbers. Typical variations of Reynolds number with Mach number for the two types of test runs are given in figure 5.

ACCURACY

The accuracy of the major variables in this investigation was estimated to be within the following limits:

Mach number	± 0.01
Angle of attack, degree	± 0.3
Flap angle, degree	± 0.3
Lift coefficient	± 0.03
Pitching-moment coefficient	± 0.015
Hinge-moment coefficient	± 0.003

Accuracies of the last three variables listed above are given for the lowest test speed; at the highest test speed, these accuracies should be approximately four times better. A large part of the loss in accuracy was attributable to shifts in instrument zeros that occurred gradually during a flight. Hence, the errors in the data appear for the most part as errors in angles of zero lift, angles of zero pitching moment, and angles of zero hinge moment. Because the data at any given Mach number were obtained within a very short period of time (less than one sec) the slopes of the various force and moment coefficient curves should be accurate to a degree approaching the instrument capabilities, which, in the present case, add up to about 2 percent at intermediate test speeds.

PRESENTATION OF RESULTS

All force and moment coefficients are presented in accordance with standard NACA conventions regarding definitions and signs. Pitching moments were measured about an axis located 18.7 percent mean aerodynamic chord forward of the leading edge of the mean aerodynamic chord.

The basic data are all presented without showing test points. This procedure has been adopted in the interests of clarity. Data obtained from the balance showed some hysteresis which was traced to unequal damping of the different electrical circuits connected with the strain gages and potentiometers. There appear to be two ways to circumvent the difficulties caused by lag due to unequal damping: one way is to eliminate the lag completely by trial-and-error adjustment of the damping of the electrical circuits; the other way is to obtain data for both increasing and decreasing angle of attack (or flap deflection) and use these two sets of data to establish a single curve that represents static conditions. The latter course was followed in obtaining the basic data shown in this investigation. Either method, of course, should lead to the same result providing the lag is not large. In the present tests the lag was relatively small and it is believed that any errors incurred from this lag are negligible.

An outline giving the order of treatment of the results and a key to the figures containing the data presented follows:

BASIC DATA

Item	Content	Figure
Lift characteristics	C_L against α ($\delta_f = 0^\circ$)	6
	C_L against α ($\delta_f = 5^\circ$)	7
	C_L against δ_f ($\alpha \approx 0^\circ$)	8
	C_L against δ_f ($\alpha \approx 5^\circ$)	9
Pitching-moment characteristics	C_m against α ($\delta_f = 0^\circ$)	10
	C_m against α ($\delta_f = 5^\circ$)	11
	C_m against δ_f ($\alpha \approx 0^\circ$)	12
	C_m against δ_f ($\alpha \approx 5^\circ$)	13
Hinge-moment characteristics	C_h against α ($\delta_f = 0^\circ$)	14
	C_h against α ($\delta_f = 5^\circ$)	15
	C_h against δ_f ($\alpha \approx 0^\circ$)	16
	C_h against δ_f ($\alpha \approx 5^\circ$)	17

SUMMARY DATA

Item	Content	Figure
Lift characteristics	$C_{L\alpha}$, $C_{L\delta}$, $\frac{\partial \alpha}{\partial \delta}$ against M ($\alpha \approx 0$; $\delta_f = 0$) Effect of δ_f on $C_{L\alpha}$ Effect of α on $C_{L\delta}$	18 19(a) 19(b)
Pitching-moment characteristics	$C_{m\alpha}$, $C_{m\delta}$, a.c., c.p. due to δ_f against M ($\alpha \approx 0$, $\delta_f = 0$) $C_{m\alpha}$, $C_{m\delta}$, a.c., c.p. due to δ_f against M ($\alpha \approx 0$, $\delta_f = 0$) (plain flap) Effect of δ_f on $C_{m\alpha}$ Effect of α on $C_{m\delta}$ Effect of δ_f on a.c. position Effect of α on c.p. due to δ_f	20 21 22(a) 22(b) 22(c)
Hinge-moment characteristics	$C_{h\alpha}$, $C_{h\delta}$ against M ($\alpha \approx 0^\circ$; $\delta = 0^\circ$) Effect of δ_f on $C_{h\alpha}$ Effect of α on $C_{h\delta}$	23 24(a) 24(b)

DISCUSSION OF RESULTS

BASIC DATA

Lift Characteristics

Lift due to angle of attack.- The variations of lift coefficient with angle of attack are shown for a flap angle of 0° in figure 6 and for a flap angle of 5° in figure 7. Curves are given, in general, for Mach number increments of 0.05 throughout the Mach number range tested. Data from the high-dive runs are given in part (a) of the figures, and for the level-flight runs in part (b) of the figures.

The lift-curve slope was practically independent of Mach number (figs. 6 and 7). A slight increase in lift-curve slope with increasing Mach number occurred at subsonic speeds in accordance with theory. At many of the Mach numbers for which data are presented, the lift-curve slope increased very slightly with increasing angle of attack. This phenomena is a characteristic of sweptback airfoils of low aspect ratio and has been found previously in low-speed wind-tunnel tests. Although it appears that maximum lift was never reached in the present tests, a preliminary stall is shown to occur at angles of attack as low as 10° for Mach numbers between 0.85 and 1.05. A comparison between figures 6 and 7 shows that there was very little effect of a 5° flap deflection on the over-all trends of the lift due to angle of attack. The preliminary stall in general occurred at a higher angle of attack with 5° flap deflection than with 0° flap deflection. Such a trend is opposite to that generally found at low speeds on conventional airfoil-flap combinations.

Tests of the plain flap (reference 1) did not reveal the existence of a preliminary stall in the lift curves; however, in that case the angle-of-attack data were of insufficient scope to define the phenomena even if it had been present.

The data of figures 8 and 9 indicate that the flap was always effective in producing lift at any speed or deflection tested. From figure 9 it is seen that with positive angle of attack the flap suffered a loss in effectiveness at small negative angles which was counterbalanced by an increase in effectiveness at large negative angles. This effect was most pronounced at a Mach number of 0.95. A close inspection of figures 8 and 9 shows that the flap effectiveness measured at zero flap angle changed noticeably with Mach number, Reynolds number, and angle of attack. These changes are given in quantitative form in a subsequent section of this investigation.

Pitching-Moment Characteristics

Pitching moment due to angle of attack.- The variations of pitching-moment coefficient with angle of attack are presented in figure 10

for 0° flap angle and in figure 11 for 5° flap angle. In general, the pitching-moment curves were smooth and showed no unusual variations. Because the pitching moments were measured about an axis approximately 40 percent mean aerodynamic chord ahead of the usual aerodynamic-center position, small changes in aerodynamic-center position did not cause appreciable changes in the shape of the pitching-moment curves.

Pitching moment due to flap deflection.- The pitching-moment coefficients resulting from flap deflection are shown for approximately 0° angle of attack in figure 12 and for approximately 5° angle of attack in figure 13. As in the case of the pitching moment and lift variations with angle of attack, the pitching moment against flap-deflection curves were similar to the lift against flap-deflection curve and showed no unusual variations. Here, also, as noted previously, changes in the location of the center of pressure due to flap deflection caused only small changes in the pitching-moment curves because of the far forward position of the axis about which pitching moments were measured. Close comparison of figures 8 and 9 with figures 12 and 13 shows that the pitching-moment coefficient due to flap deflection dropped off faster with increasing flap deflection than the lift coefficient did. Such a trend means that the center of pressure due to flap deflection moves forward at large flap deflections; this effect appeared to be largely independent of Mach number.

Hinge-Moment Characteristics

Hinge moment due to angle of attack.- Hinge-moment coefficient variations with angle of attack are shown in figure 14 for a flap angle of 0° and in figure 15 for a flap angle of 5° . At speeds below a Mach number of about 0.95 with zero flap angle (figs. 14(a) and 14(b)) the slopes of the hinge-moment curves at 0° angle of attack were always positive indicating a tendency of the flap to float against the relative wind. Such a result is not surprising in view of the fact that the plain flap of reference 1 showed no floating tendency at 0° angle of attack over the same Mach number range. Above $M = 0.95$ the horn-balanced flap always tended to float with the relative wind. The change in floating tendency in a negative direction as the speed increases from subsonic to supersonic is believed to be a feature common to all trailing-edge controls on conventional wings because the centers of pressure of supersonic lift distributions are, as a rule, farther rearward than those of subsonic lift distributions. Comparison between figures 14(a) and 14(b) indicates slight changes were caused by changes in Reynolds number but the important characteristics are duplicated in the data from both the high-dive and level-flight runs. It may be noted that the hinge moment was not zero when both the angle of attack and the flap deflection were zero. This is attributed to a very slight lateral misalignment of the flap behind the fixed portion of the model. The flap hinge line was slightly toward the model upper surface in the spanwise region of the tip.

When the flap was deflected 5° (figs. 15(a) and 15(b)) the floating tendency at low speeds at 0° angle of attack was approximately zero. The change from the zero flap-angle case may have been caused by flow separation on the protruding horn. In this configuration also, a strong negative floating tendency appeared as sonic speed was exceeded.

Hinge moment due to flap deflection.- Measured variations of hinge-moment coefficient with flap deflection are shown for approximately 0° angle of attack in figure 16 and for approximately 5° angle of attack in figure 17. Below a Mach number of 0.90, at approximately 0° angle of attack (fig. 16), the horn provided nearly uniform balancing for flap deflections of $\pm 10^\circ$. Above a Mach number of 0.90, hinge moments due to deflection increased in magnitude very rapidly. The effect of increasing the angle of attack to 5° (fig. 17) was to shift the region of high balance at low speeds so that it was centered around a negative flap deflection of 5° - the deflection at which the horn was lined up with the relative wind. It is thought that the balancing effectiveness of the horn might be extended to higher flap deflections if the inboard edges of the horn were rounded instead of being squared off as in the present tests. Low-speed tests (reference 2) indicate such rounding off would also change the balancing effectiveness at small deflections. Comparison between the parts (a) and (b) of figures 16 and 17 indicates Reynolds number had some effects on the hinge-moment characteristics but these effects were of a minor nature.

SUMMARY DATA

Lift Characteristics

Lift-curve slope.- The variations of C_{L_α} with Mach number are shown in figure 18. Although there was a small increase in lift-curve slope with increasing Mach number at subsonic speeds as would be expected from theory, for all practical purposes the lift-curve slope was independent of Mach number. The small variations in lift-curve slope with Mach number that did exist nearly duplicated the trends found in previous tests of a plain flap; however, the numerical values of lift-curve slope were, on an average, 12 percent less for the model with horn-balanced flap. This loss in lift-producing ability is attributed largely to the injurious effect of pressure equalization through the gap at the inboard edge of the horn balance. Because it is exceedingly difficult to seal this gap, the horn-type balance may prove to be undesirable in cases where the maximum lift due to angle of attack is required. Reynolds number had a more pronounced effect on the lift-curve slopes of the horn-balanced model than of the plain flap model. Figure 18 indicates the lift-curve slopes for the high-dive and level flight runs differed by from 2 to 10 percent; however, some of this scatter might have been caused by experimental error particularly at the lower speeds.

The effect of flap deflection on the lift-curve slopes at 0° angle of attack is shown in figure 19(a). The lift-curve slope was nearly always less with the flap deflected 5° than with the flap in neutral. This trend might have been caused by flow separation over the horn resulting in loss of lift in the flap-deflected condition.

Flap effectiveness.- Absolute flap effectiveness $C_{L\delta}$ measured at α approximately 0° , $\delta = 0^\circ$ is plotted as a function of Mach number in figure 18. These data show that the flap lost effectiveness as the speed was increased to $M = 0.95$; above $M = 1.0$ there was slight recovery in absolute effectiveness. The effectiveness of the horn-balanced flap was nearly identical to that of the plain flap of reference 1 at Mach numbers above 1.0; at Mach numbers below 1.0 the horn-balanced flap always showed lower effectiveness than the plain flap. Furthermore, the effectiveness of the horn-balanced flap definitely was dependent on Reynolds number whereas this was not the case with the plain flap. When the angle of attack was raised to 5° (fig. 19(b)), the absolute effectiveness of the horn-balanced flap increased very noticeably, was much less dependent on Reynolds number, and, was nearly identical at all test speeds to the effectiveness of the plain flap measured also for $\alpha = 5^\circ$.

Relative flap effectiveness $\partial\alpha/\partial\delta$ is also shown in figure 18. Below a Mach number of 0.90 the relative flap effectiveness of the horn-balanced flap was the same as that of the plain flap even though both the lift-curve slope and the absolute flap effectiveness were less. Above a Mach number of 1.0 the relative flap effectiveness of the horn-balanced flap was slightly greater than that of the plain flap, largely because the lift-curve slope was lower. Such trends as these indicate why the parameter $\partial\alpha/\partial\delta$ may be very misleading if it is interpreted too literally as "flap effectiveness" in cases where no information regarding actual lift is available.

Pitching-Moment Characteristics

Pitching-moment coefficient per degree angle of attack.- The pitching-moment slopes $C_{m\alpha}$ at zero lift ($\alpha \approx 0$; $\delta_p = 0$) are plotted against Mach number at the top of figure 20. For purposes of comparison, the plain-flap pitching-moment data are presented in figure 21. The slopes of the pitching-moment curves for the horn-balanced flap (fig. 20) did not change appreciably with change in Mach number and, like the lift-curve slopes, were relatively insensitive to the changes in Reynolds number encountered. The effect of flap deflection on the pitching-moment variation with angle of attack is shown in figure 22(a). Only small changes in $C_{m\alpha}$ resulted from deflecting the flap 5° and these changes were apparently dependent on Reynolds number at speeds below $M = 0.90$. Above $M = 0.90$, there was a definite tendency for $C_{m\alpha}$ to increase with increasing flap deflection.

Pitching moment per degree flap deflection.- Curves of $C_{m\delta}$ measured at approximately zero lift ($\alpha \approx 0^\circ$; $\delta = 0^\circ$) are also shown near the top of figure 20. The pitching moment per degree flap angle did not change appreciably with Mach number over the range tested. However, like the lift per degree flap deflection $C_{L\delta}$ the pitching moment per degree deflection was definitely dependent on Reynolds number at zero lift. When the angle of attack was raised to about 5° (fig. 22(b)) the parameter $C_{m\delta}$ increased appreciably and became less dependent on Reynolds number in much the same manner as the parameter $C_{L\delta}$. Such similarity, of course, should be expected because in the present tests, the pitching moment was a reflection of the lift so long as the center of pressure did not move appreciably.

Aerodynamic-center location.- The positions of the aerodynamic center at $\alpha \approx 0^\circ$, $\delta_f = 0^\circ$ are plotted as a function of Mach number in figure 20. The aerodynamic center was at approximately 23 percent mean aerodynamic chord at speeds below $M = 0.95$. Starting at $M = 0.95$, the aerodynamic center moved rearward gradually from 23 percent to 31 percent mean aerodynamic chord at $M = 1.10$. Above $M = 1.10$ the data indicate the aerodynamic center tended to shift forward again. Comparison between figures 20 and 21 shows that the aerodynamic center of the horn-balanced flap model was farther rearward than that of the plain flap model at Mach numbers below 0.90. At Mach numbers above 0.95, the aerodynamic centers of the two models were almost identical. The different aerodynamic-center positions found for the horn-balanced model at low speeds are evidently attributable to the existence of the gap at the inboard edge of the horn since this gap constitutes the only physical difference between the two models that could reasonably affect the lift characteristics. The effect of flap deflection on aerodynamic-center location (fig. 22(c)) generally was to move the aerodynamic center farther rearward particularly at speeds above $M = 0.90$.

Center of pressure due to flap deflection.- Figure 20 shows also the position of the center of pressure due to flap deflection corresponding to zero lift conditions ($\alpha \approx 0^\circ$; $\delta_f = 0^\circ$). The center of pressure moved rearward more or less gradually from about 60 to 100 percent mean aerodynamic chord over the test Mach number range ($M = 0.55$ to $M = 1.10$). Such a large rearward movement suggests an outboard shift in the spanwise center of pressure due to flap deflection as well as a rearward shift of the section center of pressure with increasing Mach number. When the angle of attack was raised from 0° to 5° (fig. 22(c)), the position of the center of pressure due to flap deflection was not affected appreciably.

Hinge-Moment Characteristics

Flap floating tendency $C_{h\alpha}$.-- The rate of change of hinge-moment coefficient with angle of attack for zero lift conditions ($\alpha \approx 0^\circ$; $\delta_f = 0^\circ$) is shown by the top two curves of figure 23. The horn-balanced flap had a relatively strong positive (against the relative wind) floating tendency at low speeds which changed to a strong negative floating tendency at supersonic speeds. The effect of Reynolds number is seen to be large - the higher test Reynolds numbers gave the greater positive floating tendencies. At a flap angle of 5° (fig. 24(a)) the parameter $C_{h\alpha}$ was very little affected by Reynolds number and in this condition the floating tendency was approximately zero at low speeds; at high speeds the floating tendency was considerably greater in a negative direction than it was for zero flap angle. The peculiar bump in the curve of $C_{h\alpha}$ against M at $M = 1.0$ did not result from experimental error; this bump is the result of the peculiar manner in which the basic hinge-moment curves change from typical subsonic variations to typical supersonic variations. (See figs. 14 and 15.) In this connection too much emphasis should not be placed on the values of hinge-moment slopes measured at zero lift when, as in the present case, the hinge-moment curves are decidedly nonlinear. Whereas these slopes are of great value in assessing the degree of balance obtained by use of a given size of aerodynamic balance, it is generally desirable to refer to the complete hinge-moment data whenever possible in design work.

Flap restoring tendency $C_{h\delta}$.-- The rate of change of hinge-moment coefficient with flap deflection for zero lift conditions ($\alpha \approx 0^\circ$; $\delta_f = 0^\circ$) is shown by the middle two curves of figure 20. Two sets of data are given for the high-dive runs. Also included are data taken from reference 1 showing the characteristics of a flap having no aerodynamic balance. The horn balance eliminated about three-quarters of the unbalanced hinge moment due to deflection at speeds below $M = 0.90$. Above $M = 0.90$ the horn lost most of its balancing capabilities so that at $M = 1.05$ the hinge moments of the horn-balanced flap were only 13 percent less than those of the plain flap. Hence, it appears the horn balance as tested will not be particularly useful for flight at supersonic speeds although it apparently does offer satisfactory balancing characteristics at any speed up to a Mach number of approximately 0.95. Figure 23 shows that the hinge moments of the horn-balanced flap were affected by Reynolds number to a moderate degree whereas the hinge moments of the plain flap were insensitive to changes in Reynolds number.

The effect of angle of attack on the parameter $C_{h\delta}$ is shown in figure 24(b). Below a Mach number of 0.90 the rate of change of hinge-moment coefficient with flap deflection was essentially unaffected by

changing the angle of attack from 0° to 5° . At Mach numbers from 0.90 to 1.15, an increased angle of attack caused a sizable loss in balance, that is, an increase in the negative values of the parameter $C_{h\delta}$.

An approximate analysis was made to determine the effects of torsional flexibility of the flap on the measured hinge-moment characteristics. This analysis indicated that the errors incurred by neglecting flap twist were small and therefore no corrections were applied to the measured hinge-moment parameters. The analysis indicated, however, that for torsional stiffnesses much less than that provided by the solid dural flap tested the effects of aeroelastic distortion might be appreciable.

CONCLUSIONS

On the basis of wing-flow tests of a horn-balanced flap on a typical low-aspect ratio sweptback airfoil model the following conclusions were drawn. Where possible these conclusions are related to results obtained previously from tests of a comparable plain-flap model.

1. The lift characteristics of the horn-balanced-flap model were similar to those of the plain-flap model; however, the lift-curve slope was, on an average, 12 percent less throughout the Mach number range tested ($M = 0.55$ to 1.15), and the flap effectiveness was somewhat lower at subsonic speeds.

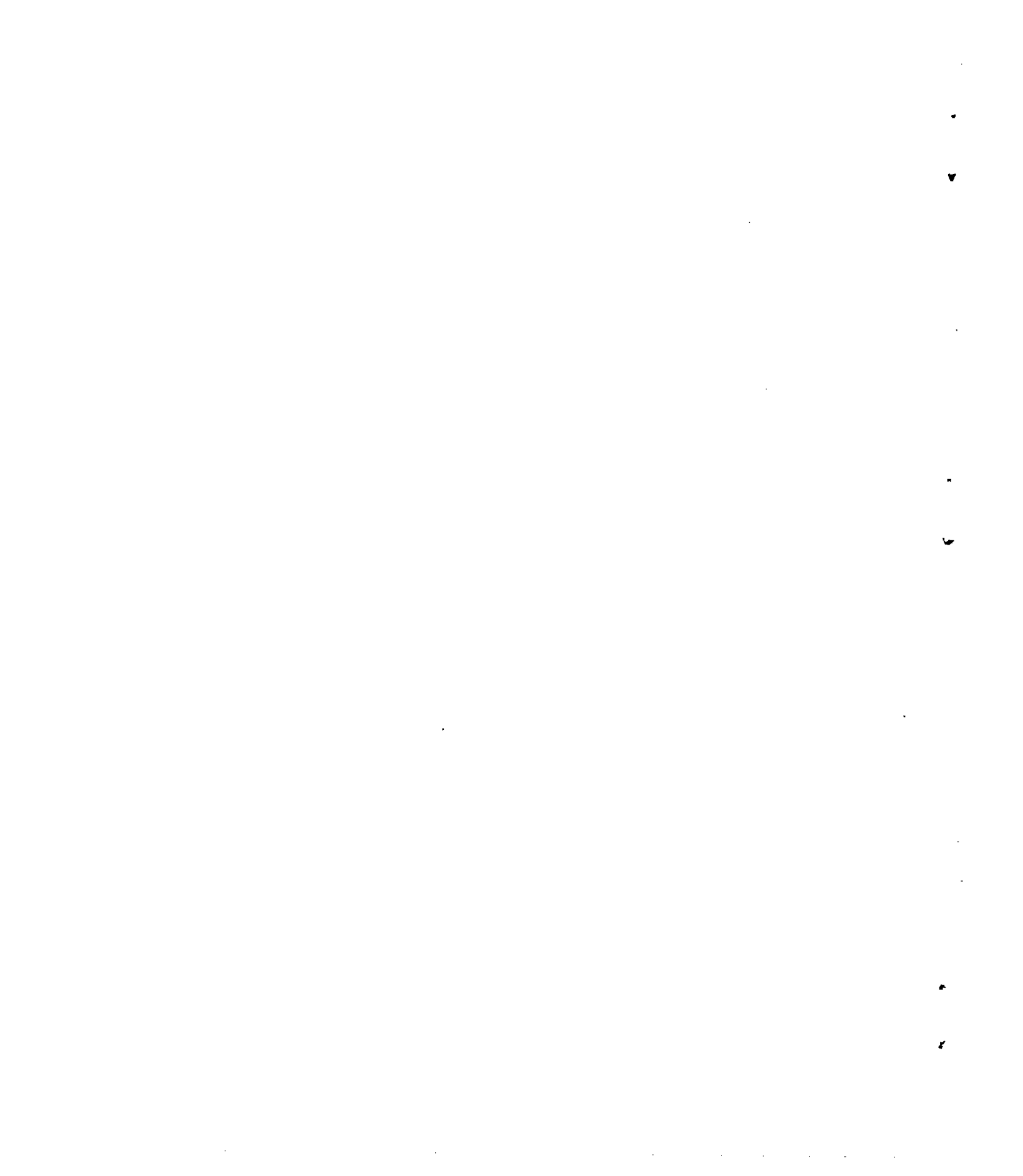
2. The horn balance eliminated approximately three-quarters of the unbalanced hinge moment due to deflection below $M = 0.90$; however, the horn apparently lost most of its balancing capabilities in passing through the speed of sound because at $M = 1.05$ the hinge moment due to deflection was only 13 percent less than that experienced by the plain flap.

3. The horn-type balance as tested appeared to offer satisfactory balancing characteristics at all speeds up to $M = 0.95$ provided that the strong positive floating tendency could be tolerated; however, the horn balance did not show promise as an effective aerodynamic balance at supersonic speeds.

Langley Aeronautical Laboratory
National Advisory Committee for Aeronautics
Langley Air Force Base, Va.

REFERENCES

1. Johnson, Harold I.: Measurements of Aerodynamic Characteristics of a 35° Sweptback NACA 65-009 Airfoil Model with $\frac{1}{4}$ -Chord Plain Flap by the NACA Wing-Flow Method. NACA RM No. L7F13, 1947.
2. Johnson, Harold S., and Thompson, Robert F.: Investigation of Horn Balances on a 45° Sweptback Horizontal Tail Surface at High Subsonic Speeds. NACA RM No. L8J01, 1948.



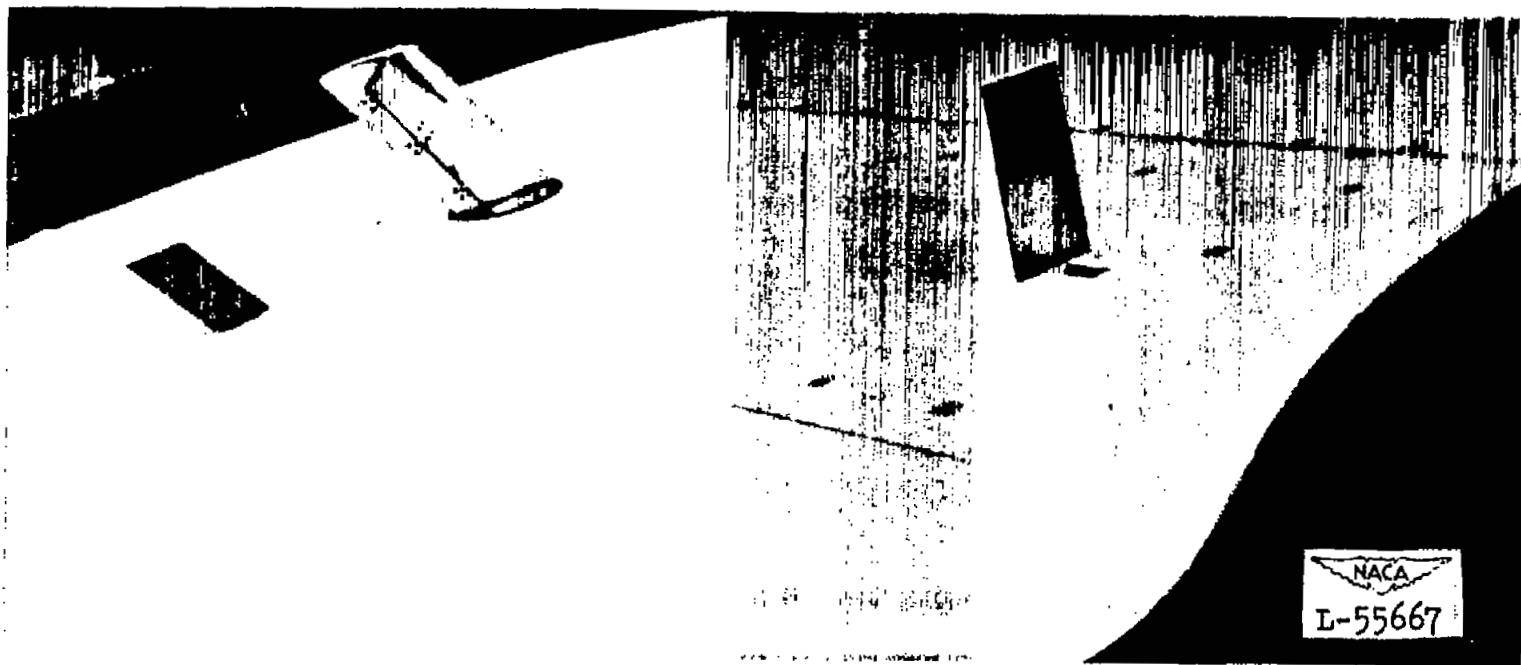


Figure 1.— View of 35° sweptback NACA 65-009 airfoil with $\frac{1}{4}$ -chord horn-balanced flap mounted on right wing of F-51D airplane. Rectangular vane on right used for measuring angle of attack. Sweptback vane on left used for measuring downwash.



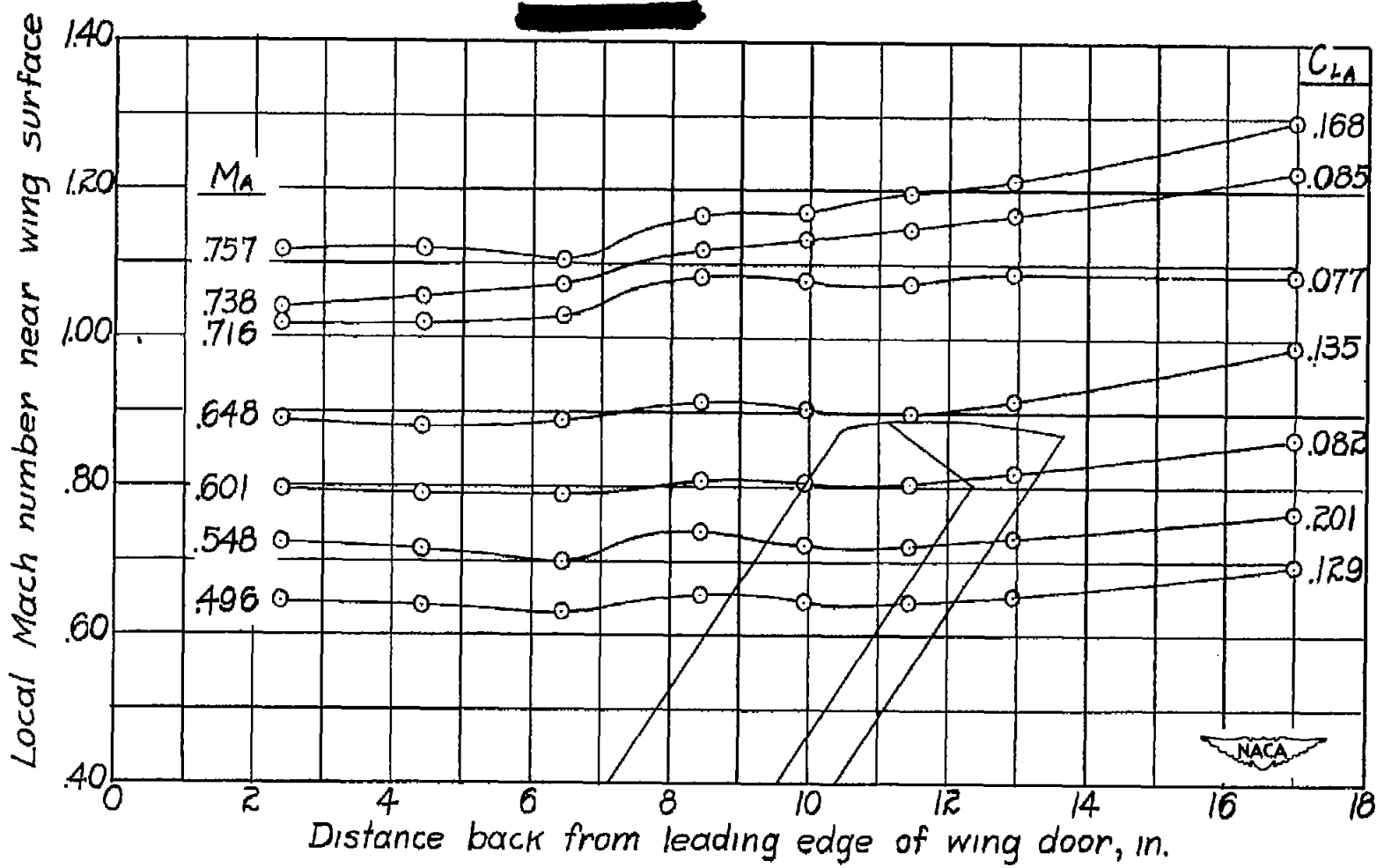


Figure 2.- Typical variations of local Mach number near wing surface with chordwise distance along wing surface for various airplane Mach numbers and lift coefficients as measured with model removed. Model location indicated by sketch.

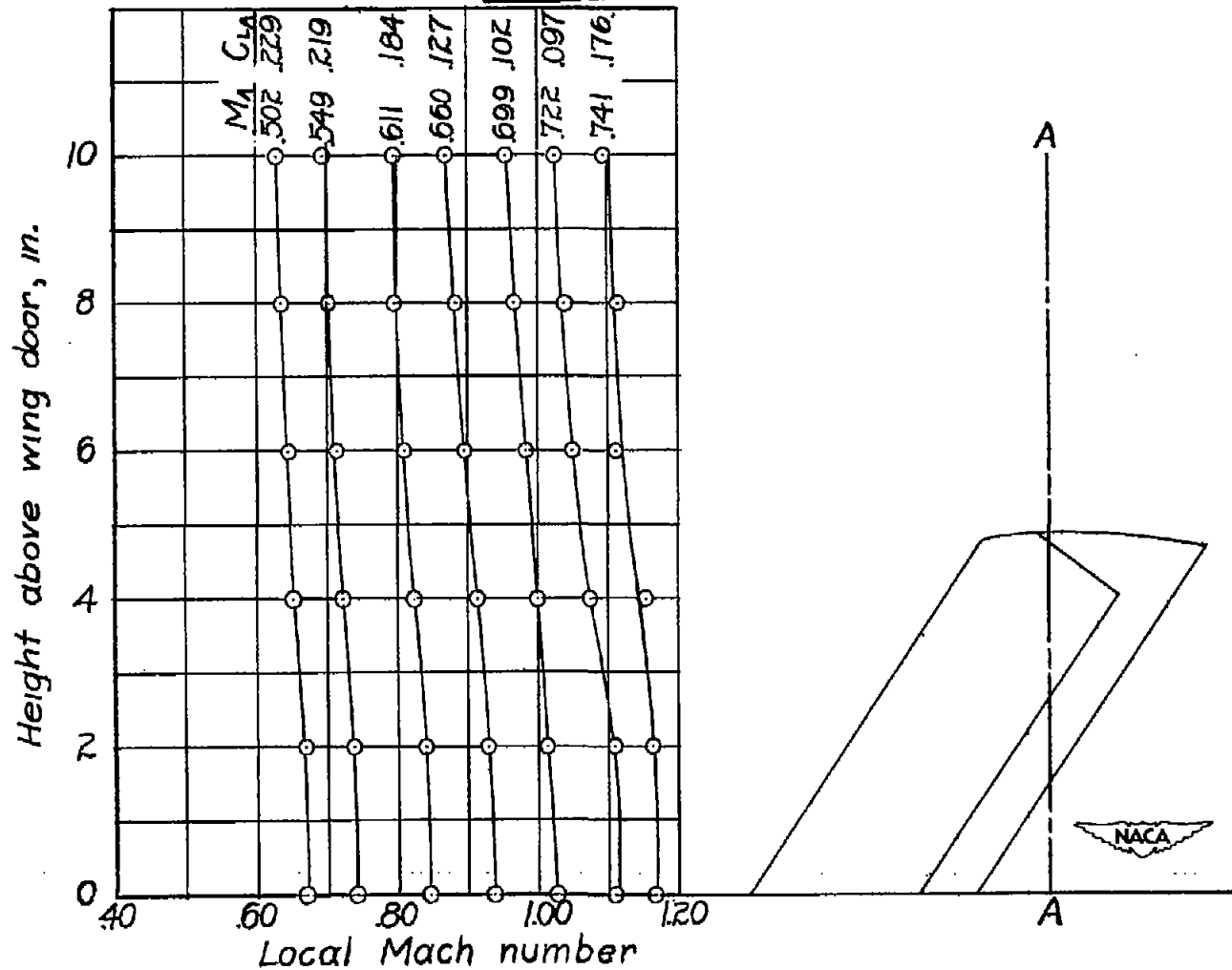


Figure 3.— Typical variations of local Mach number with vertical distance above wing surface as measured at chordwise station AA with model removed. Measurements made on left wing which had same contour as right wing. No allowance made for wing boundary layer.

$\Lambda = 35^\circ$
 $\lambda = 1.0$
 $A = 3.04$
 $b = 4.89 \text{ in.}$
 $\bar{c} = 3.27 \text{ in.}$
 $S = 15.75 \text{ in.}^2$

$b_f = 5.88 \text{ in.}$
 $c_f = \frac{1}{4} c$
 $\bar{c}_f = .564 \text{ in.}$
 $S_f = 3.87 \text{ in.}^2$
 $\phi \approx 6.0 \text{ deg}$

$\bar{c}_H = .85 \text{ in.}$
 $S_H = .73 \text{ in.}^2$
 $S_H/S_f = .189$
 $B = .491$

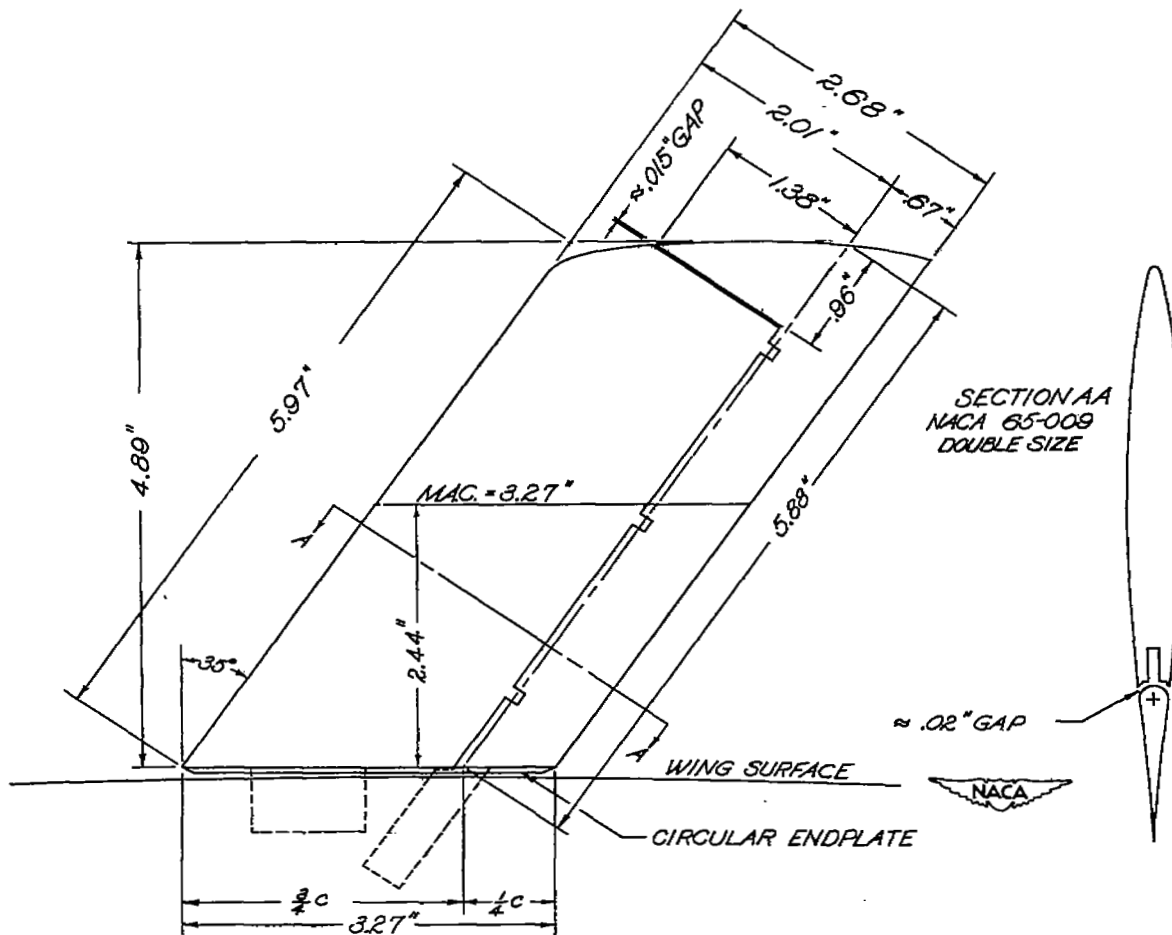


Figure 4.— Plan form and cross section of 35° sweptback NACA 65-009 airfoil with 25 percent chord unsealed, horn-balanced flap.

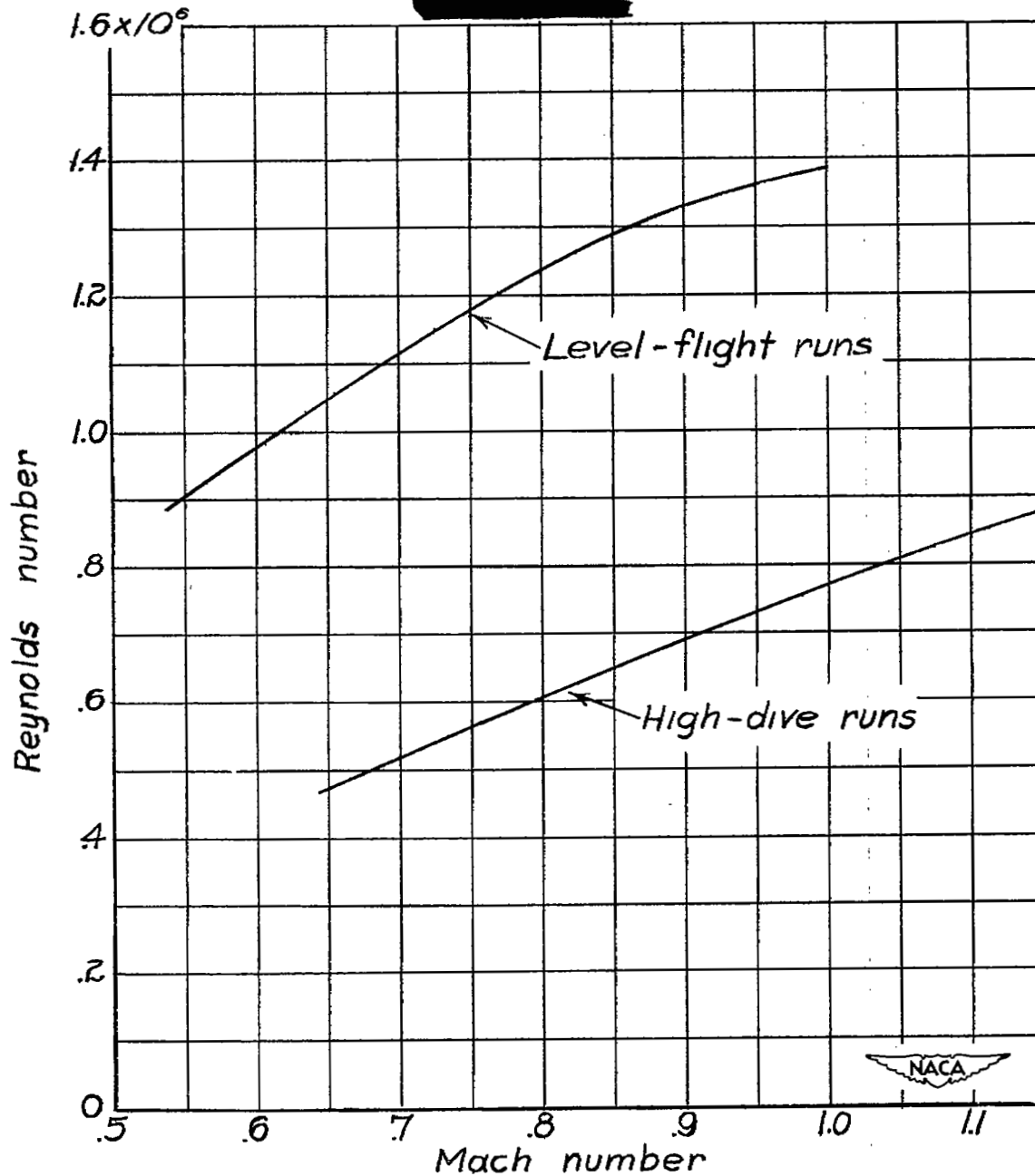
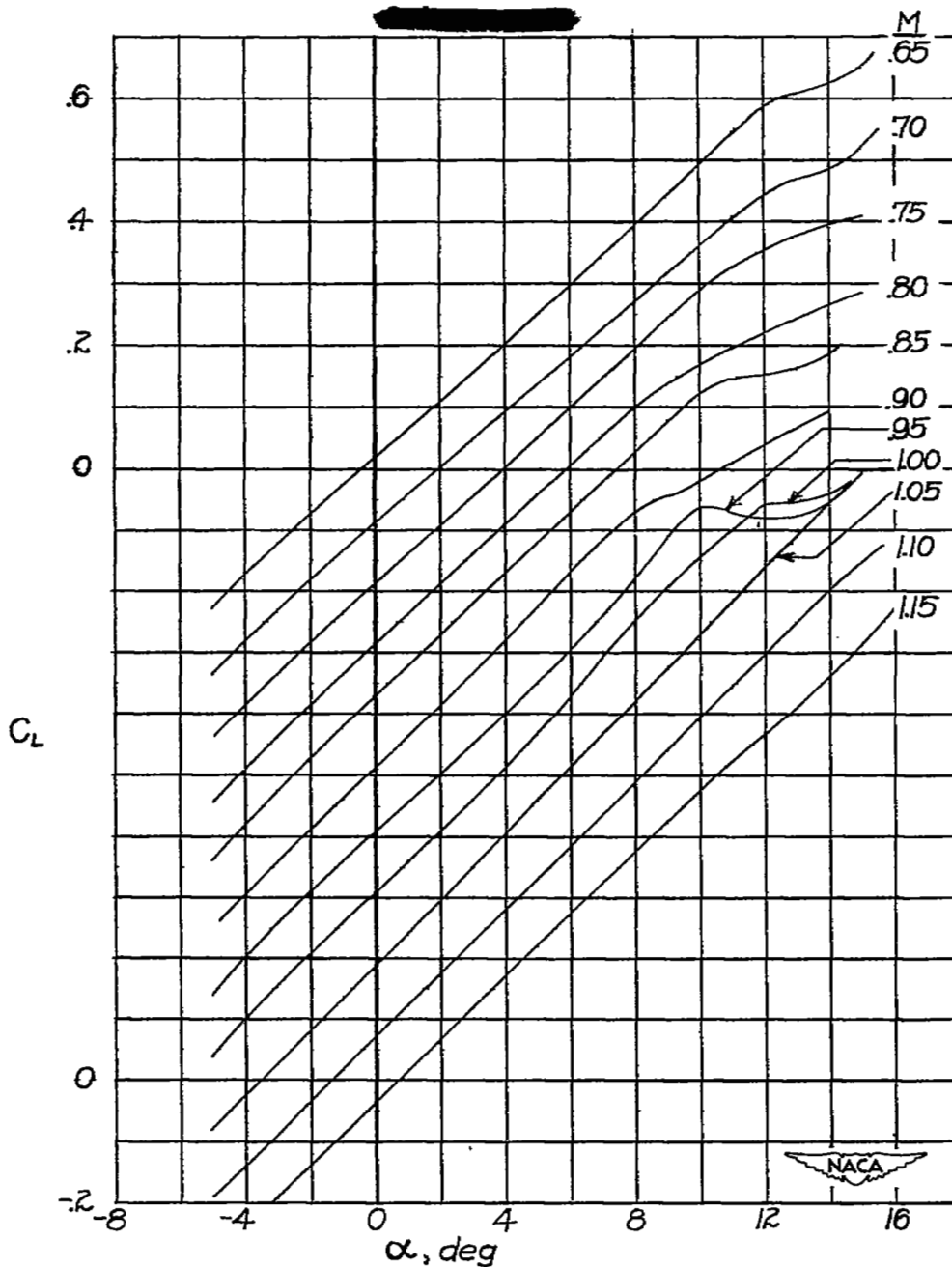
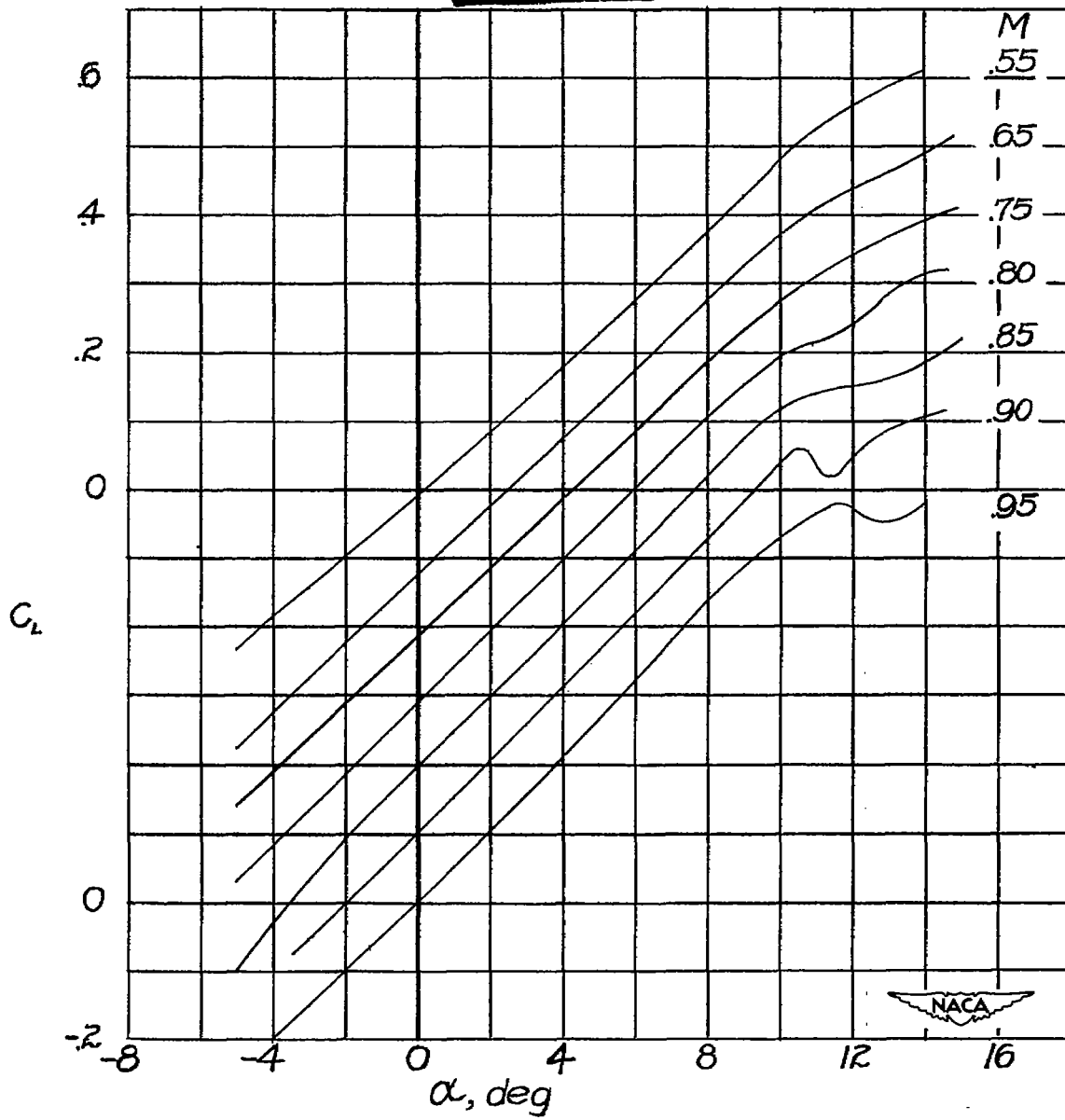


Figure 5.- Variation of Reynolds number with Mach number for tests of 35° sweptback, NACA 65-009 airfoil model with $\frac{1}{4}$ -chord horn-balanced flap by the wing-flow method. Reynolds number based on airfoil chord parallel to direction of flow.



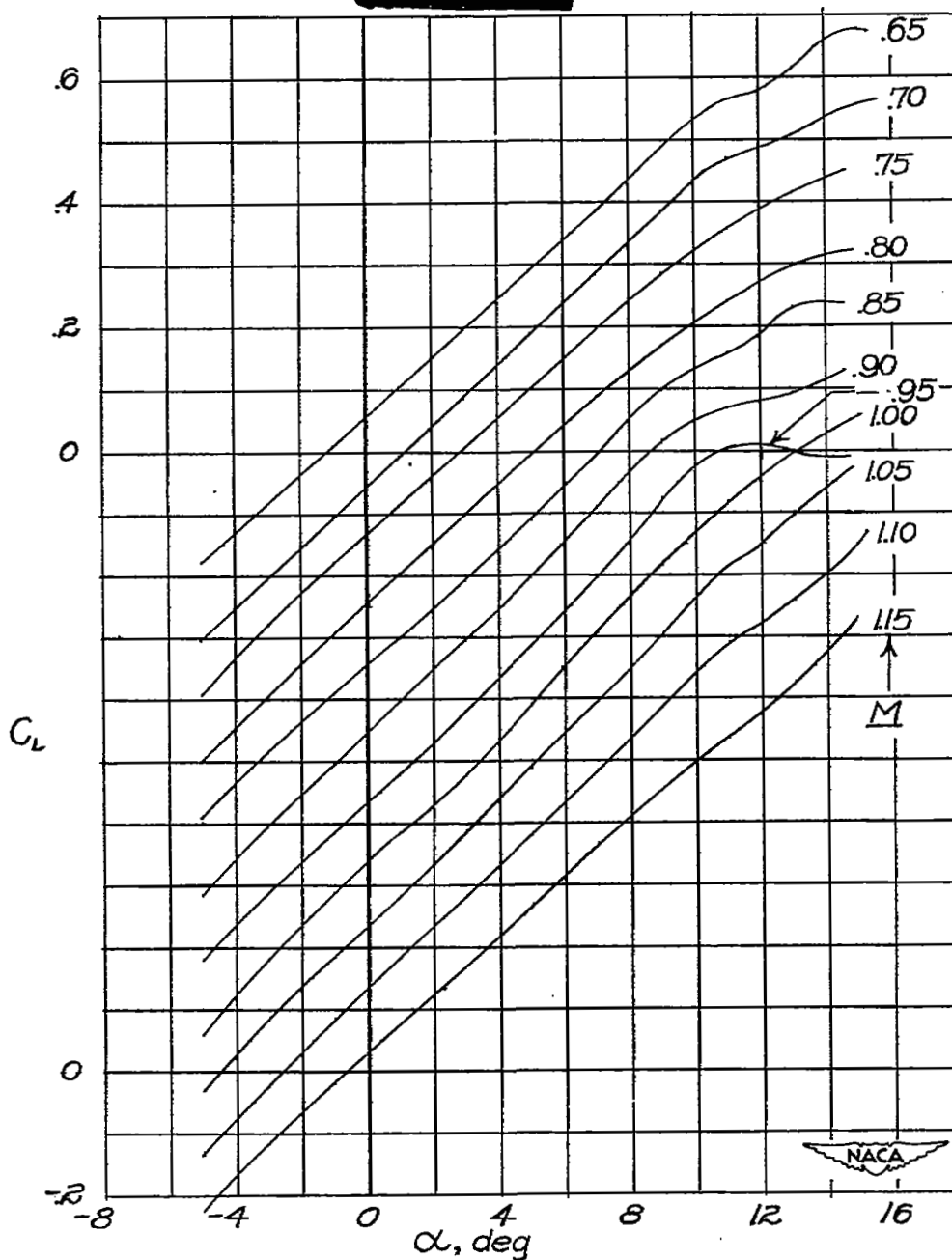
(a) High-dive runs.

Figure 6.- Variation of lift coefficient with angle of attack throughout Mach number range tested for $\delta_f = 0^\circ$. NACA 65-009 airfoil; $A = 3.04$; $\Lambda = 35^\circ$; $c_f = 0.25c$; gap unsealed; horn-balanced flap. Note shift in axis of ordinate scale for different Mach numbers.



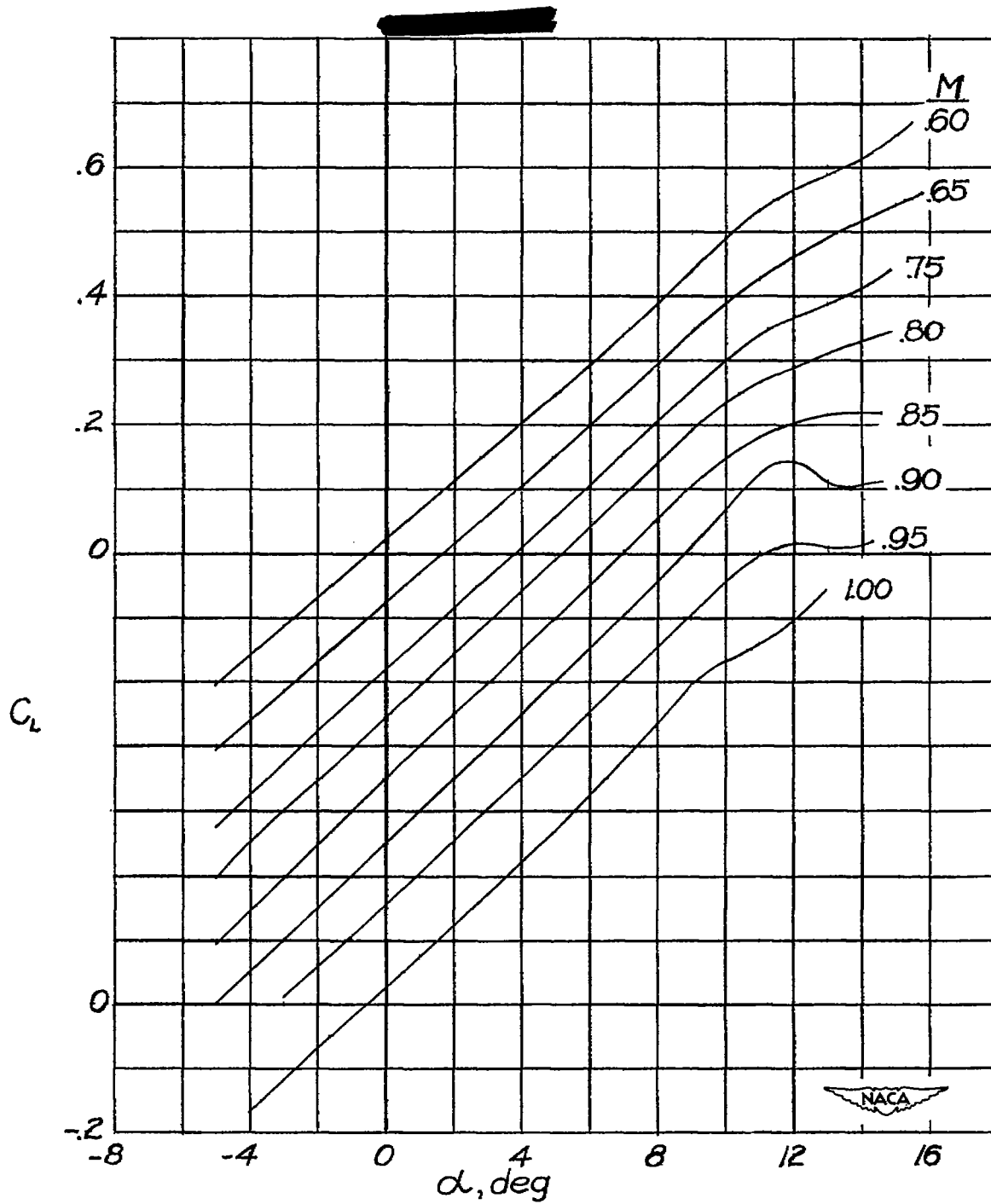
(b) Level-flight runs.

Figure 6.- Concluded.



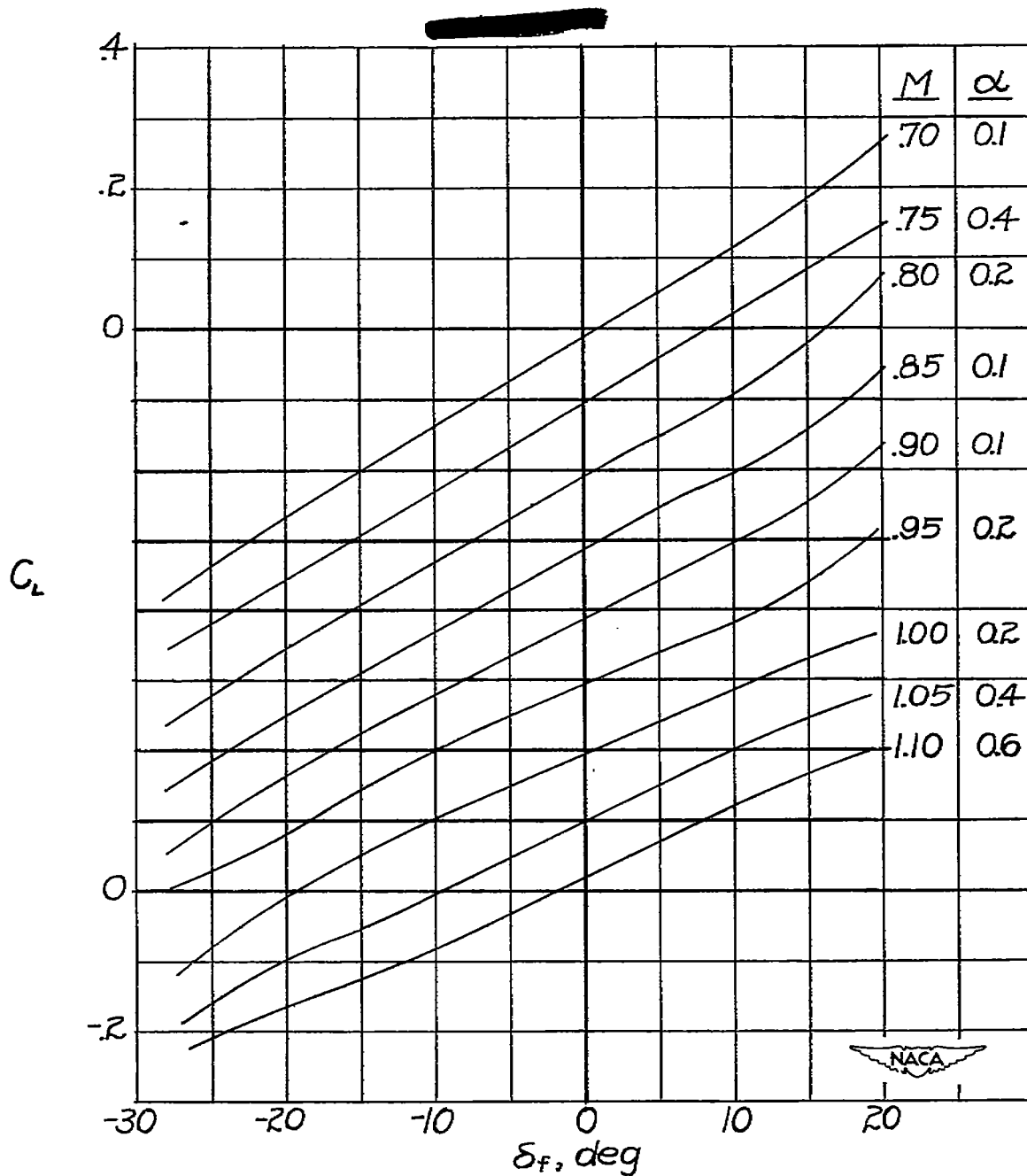
(a) High-dive runs.

Figure 7.- Variation of lift coefficient with angle of attack throughout Mach number range tested for $\delta_f = 5^\circ$. NACA 65-009 airfoil; $A = 3.04$; $\Lambda = 35^\circ$; $c_f = 0.25c$; gap unsealed; horn-balanced flap. Note shift in axis of ordinate scale for different Mach numbers.



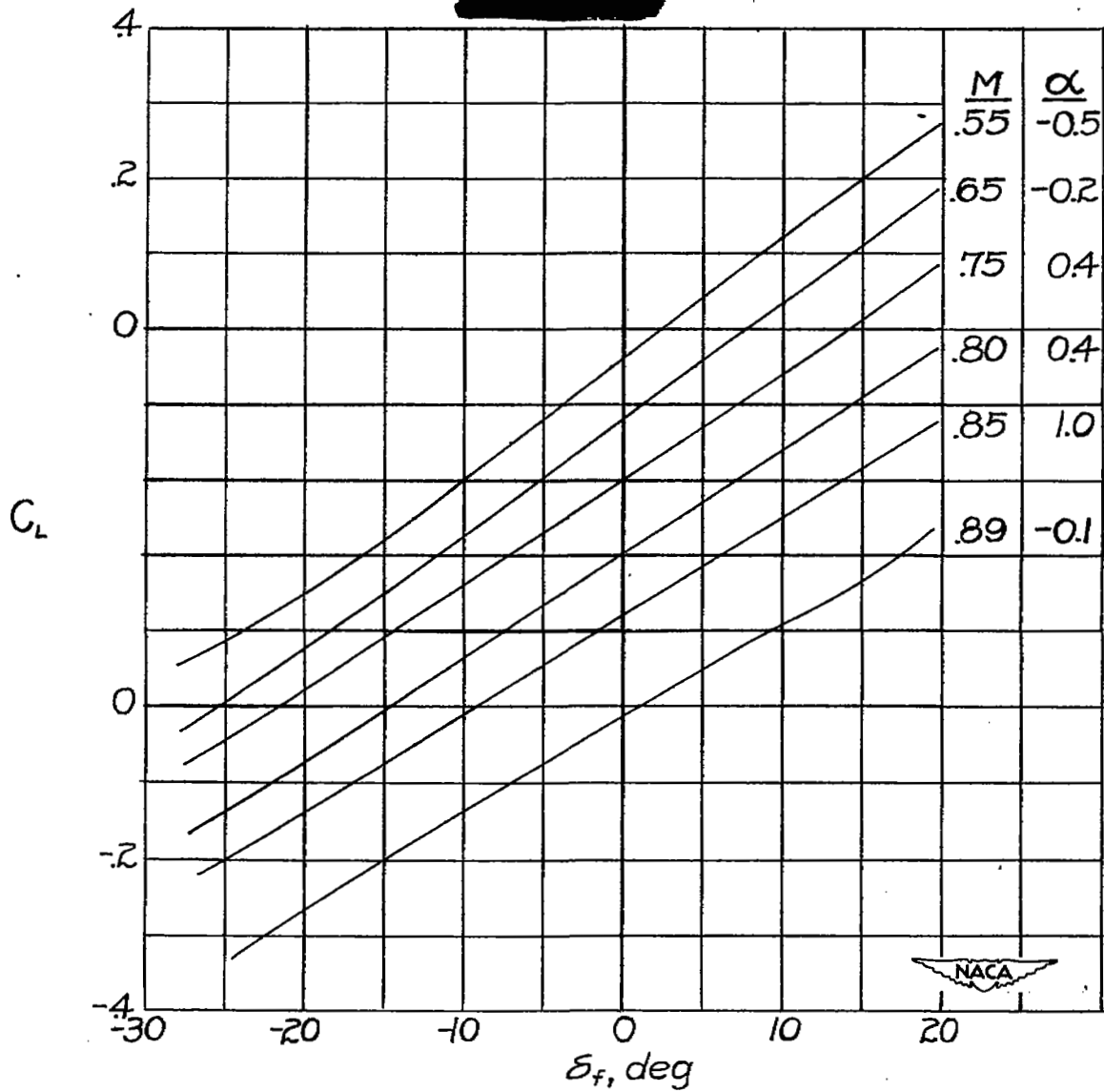
(b) Level-flight runs.

Figure 7.- Concluded.



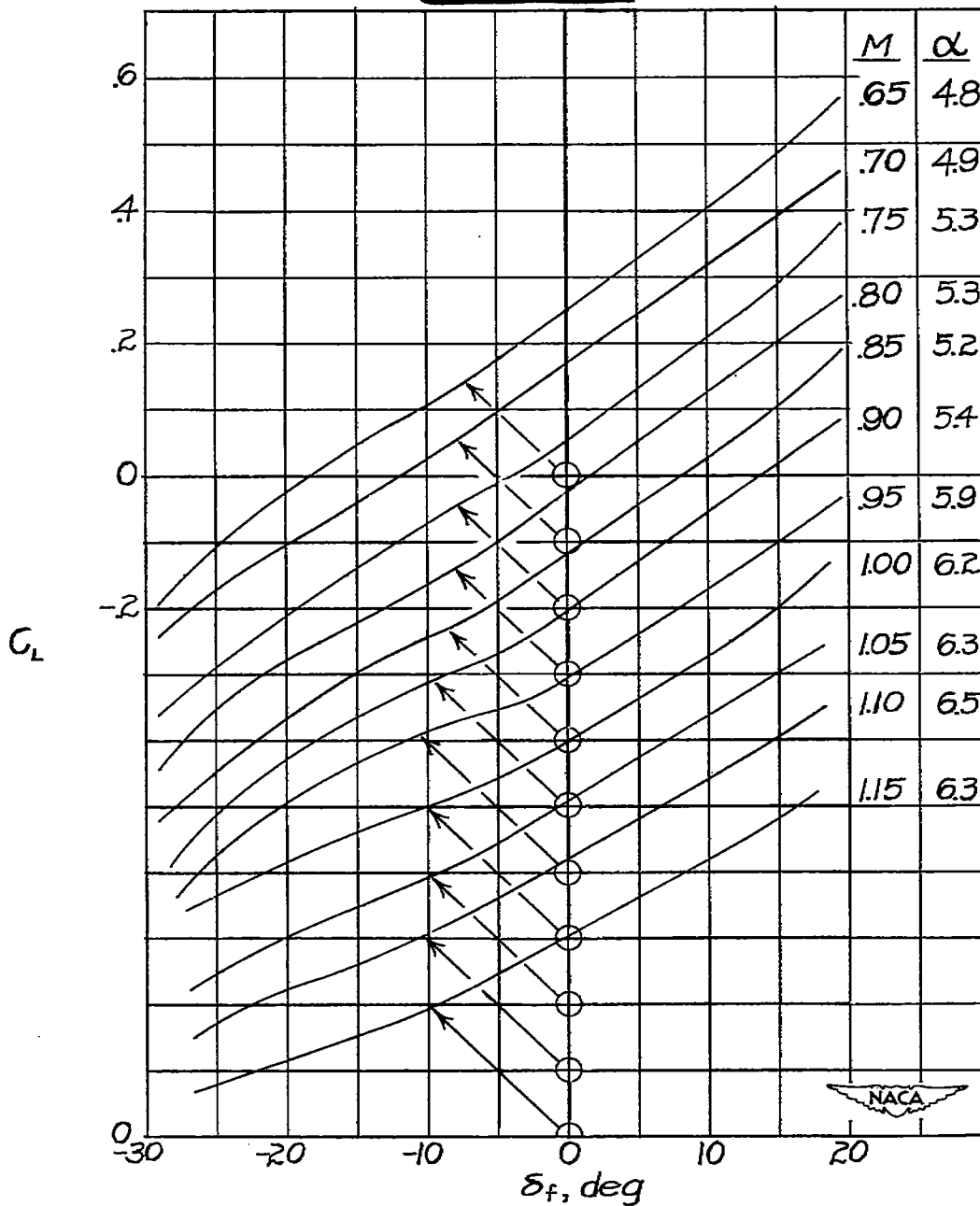
(a) High-dive runs.

Figure 8.— Variation of lift coefficient with flap deflection throughout Mach number range tested for $\alpha \approx 0^\circ$. NACA 65-009 airfoil; $A = 3.04$; $\Lambda = 35^\circ$; $c_f = 0.25c$; gap unsealed; horn-balanced flap. Note shift in axis of ordinate scale for different Mach numbers.



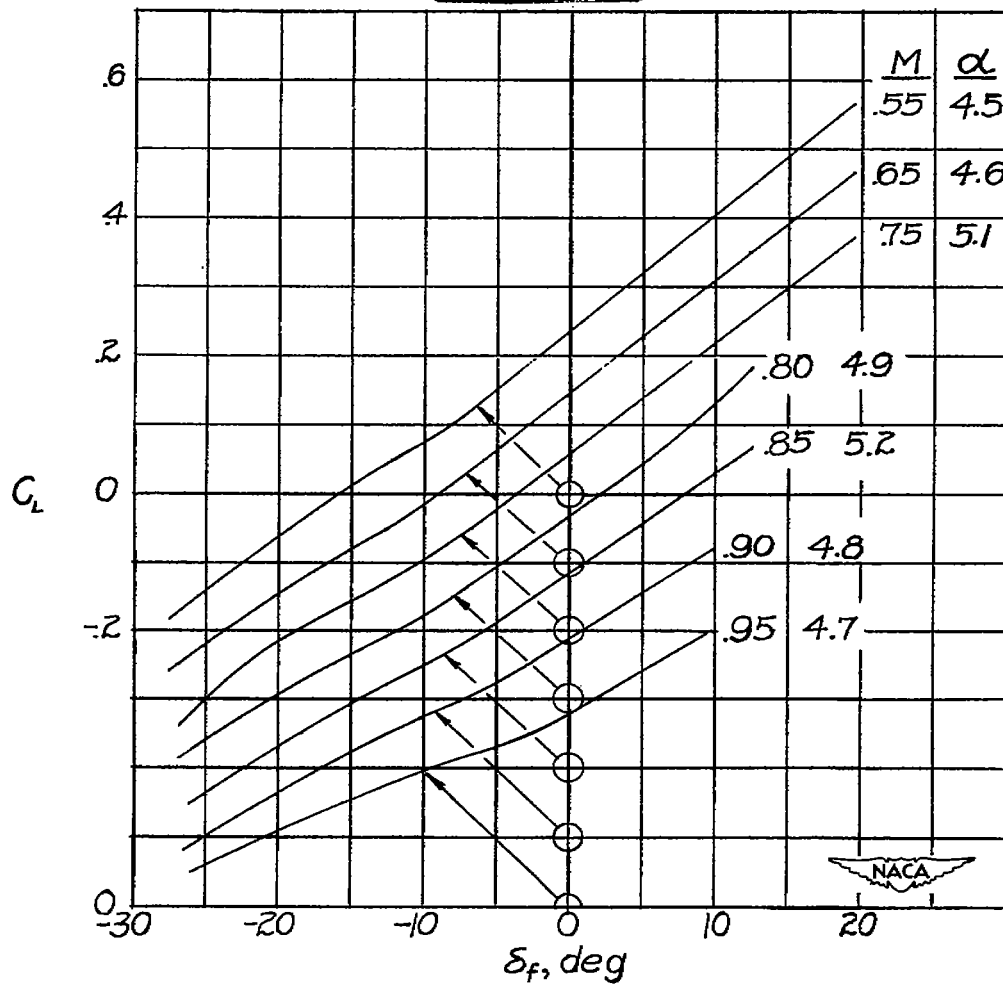
(b) Level-flight runs.

Figure 8.- Concluded.



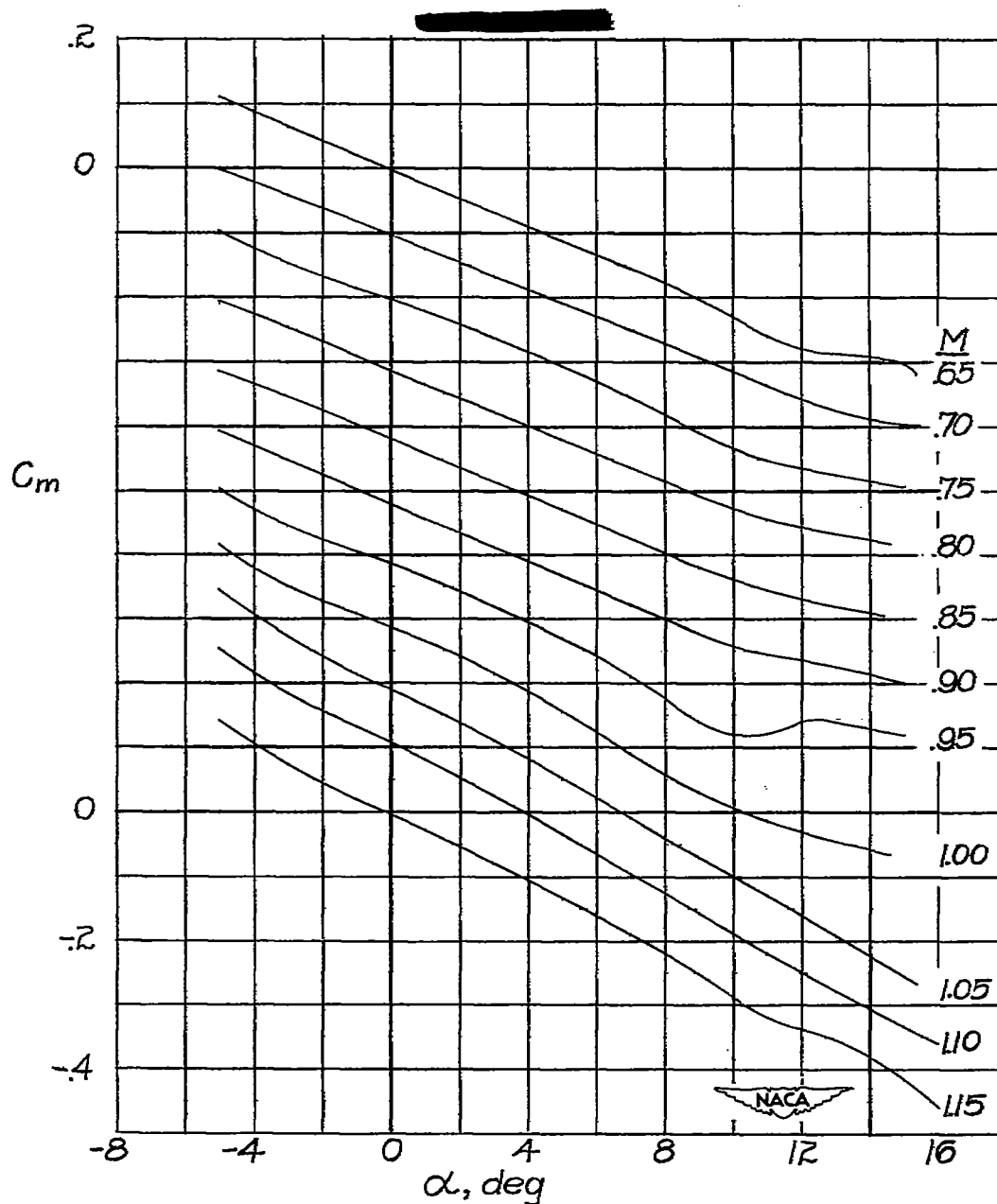
(a) High-dive runs.

Figure 9.— Variation of lift coefficient with flap deflection throughout Mach number range tested for $\alpha \approx 5^\circ$. NACA 65-009 airfoil; $A = 3.04$; $\Lambda = 35^\circ$; $c_f = 0.25c$; gap unsealed; horn-balanced flap. Note shift in axis of ordinate scale for different Mach numbers.



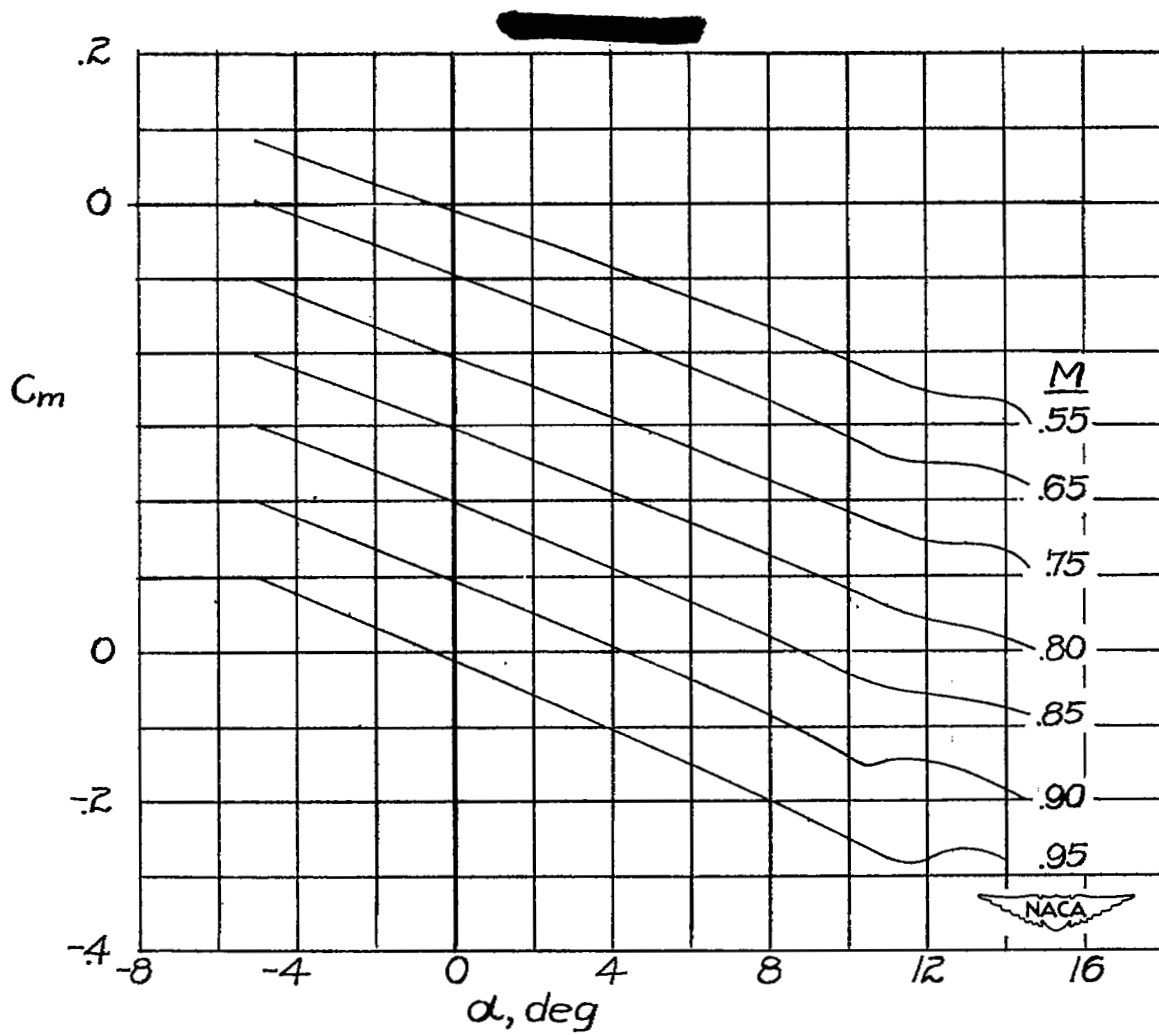
(b) Level-flight runs.

Figure 9.- Concluded.



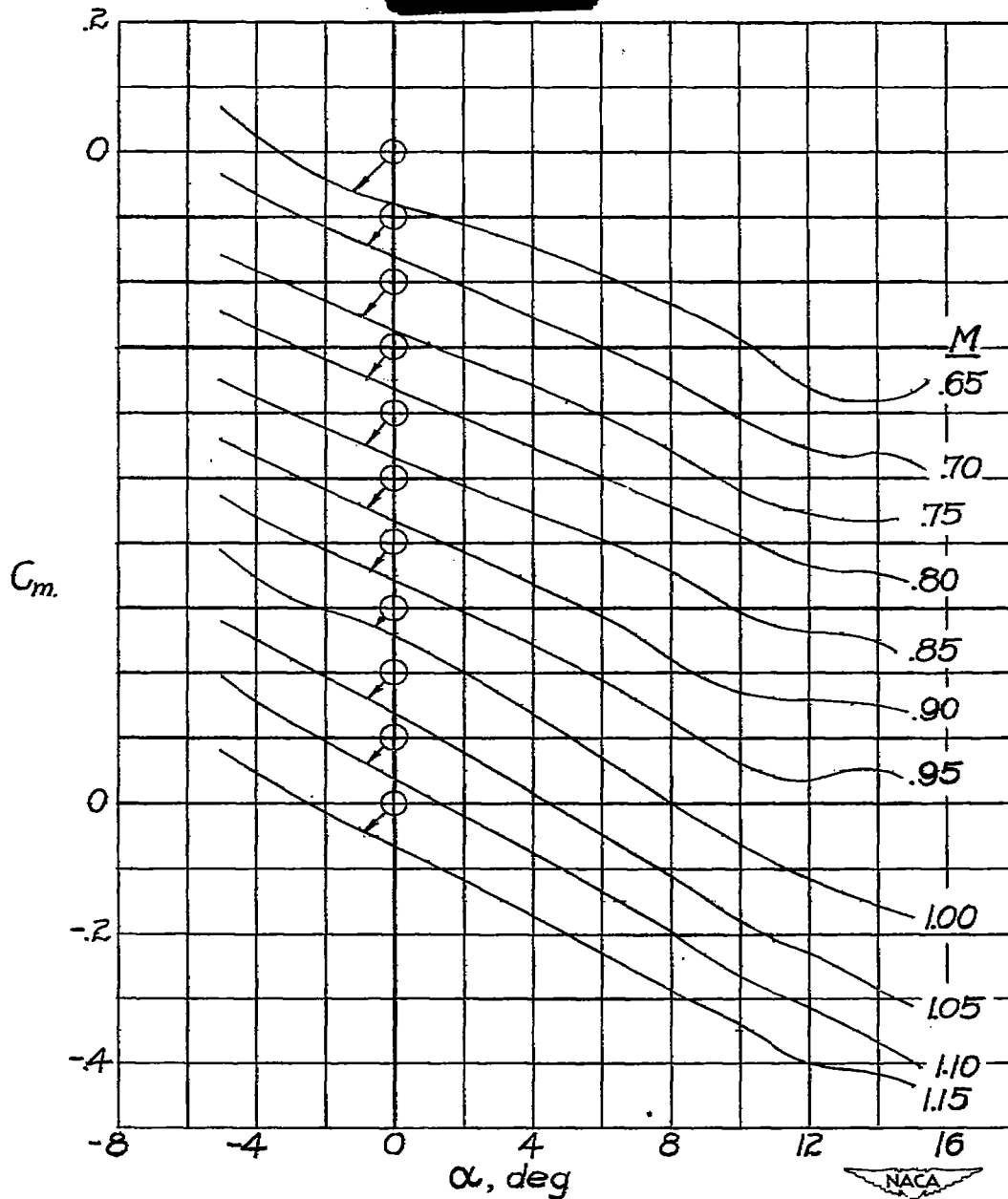
(a) High-dive runs.

Figure 10.— Variation of pitching-moment coefficient with angle of attack throughout Mach number range tested for $\delta_f = 0^\circ$. NACA 65-009 airfoil; $A = 3.04$; $\Lambda = 35^\circ$; $c_f = 0.25c$; gap unsealed; horn-balanced flap. Moment coefficient given about axis located 18.7 percent mean aerodynamic chord ahead of leading edge of mean aerodynamic chord. Note shift in axis of ordinate scale for different Mach numbers.



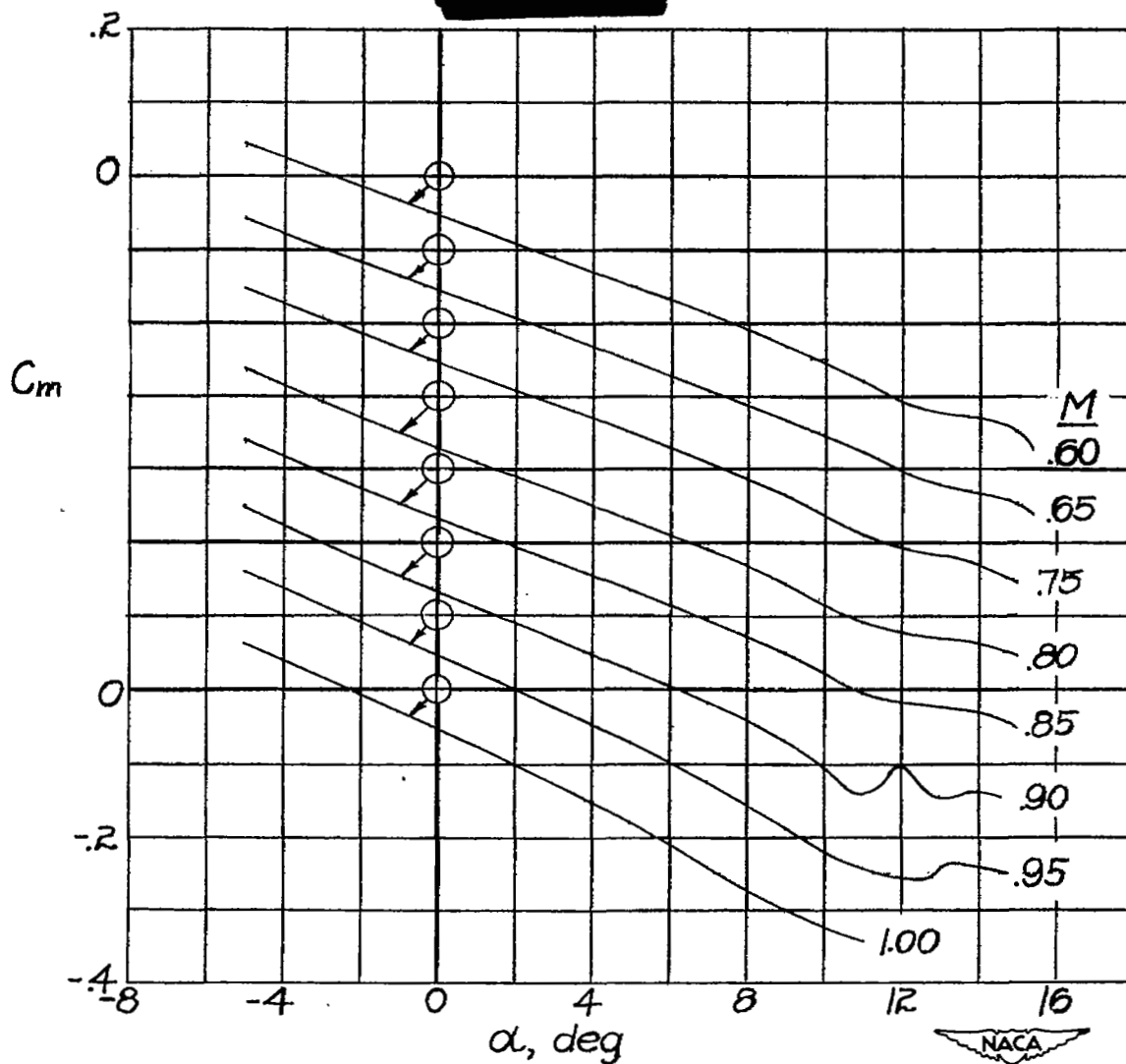
(b) Level-flight runs.

Figure 10.- Concluded.



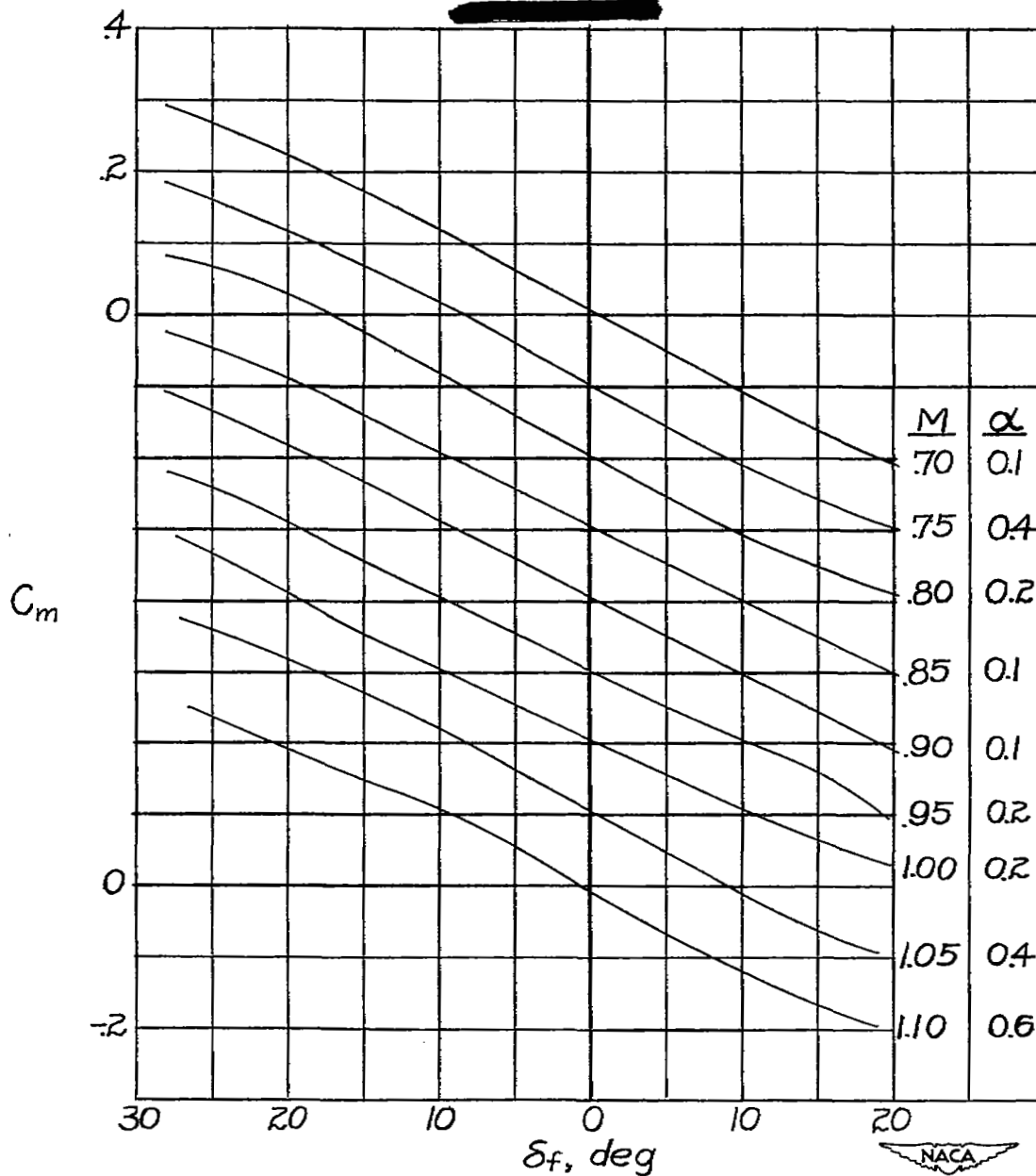
(a) High-dive runs.

Figure 11.— Variation of pitching-moment coefficient with angle of attack throughout Mach number range tested for $\delta_f = 5^\circ$. NACA 65-009 airfoil; $A = 3.04$; $\Lambda = 35^\circ$; $c_f = 0.25c$; gap unsealed; horn-balanced flap. Moment coefficient given about axis located 18.7 percent mean aerodynamic chord ahead of leading edge of mean aerodynamic chord. Note shift in axis of ordinate scale for different Mach numbers.



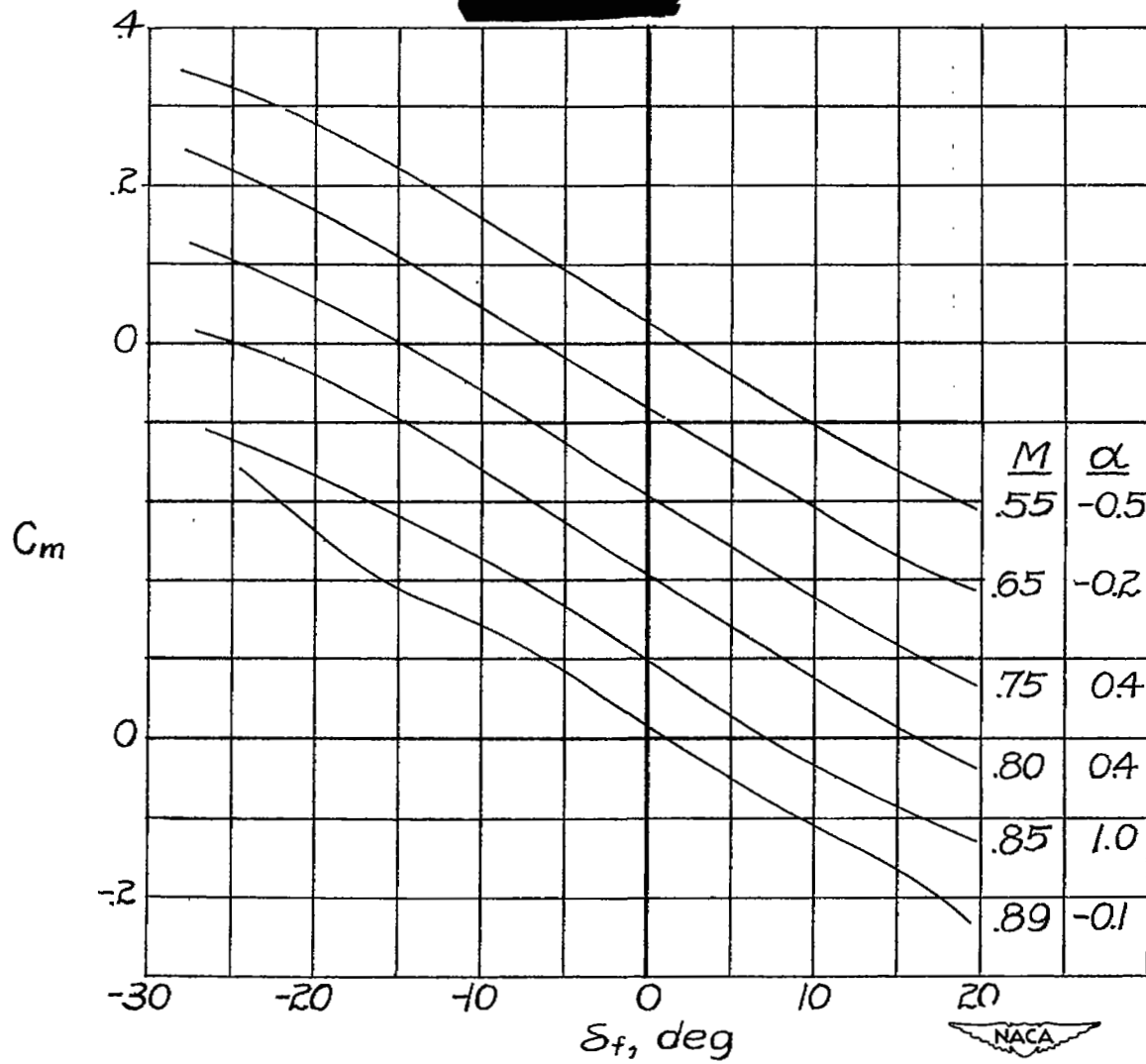
(b) Level-flight runs.

Figure 11.- Concluded.



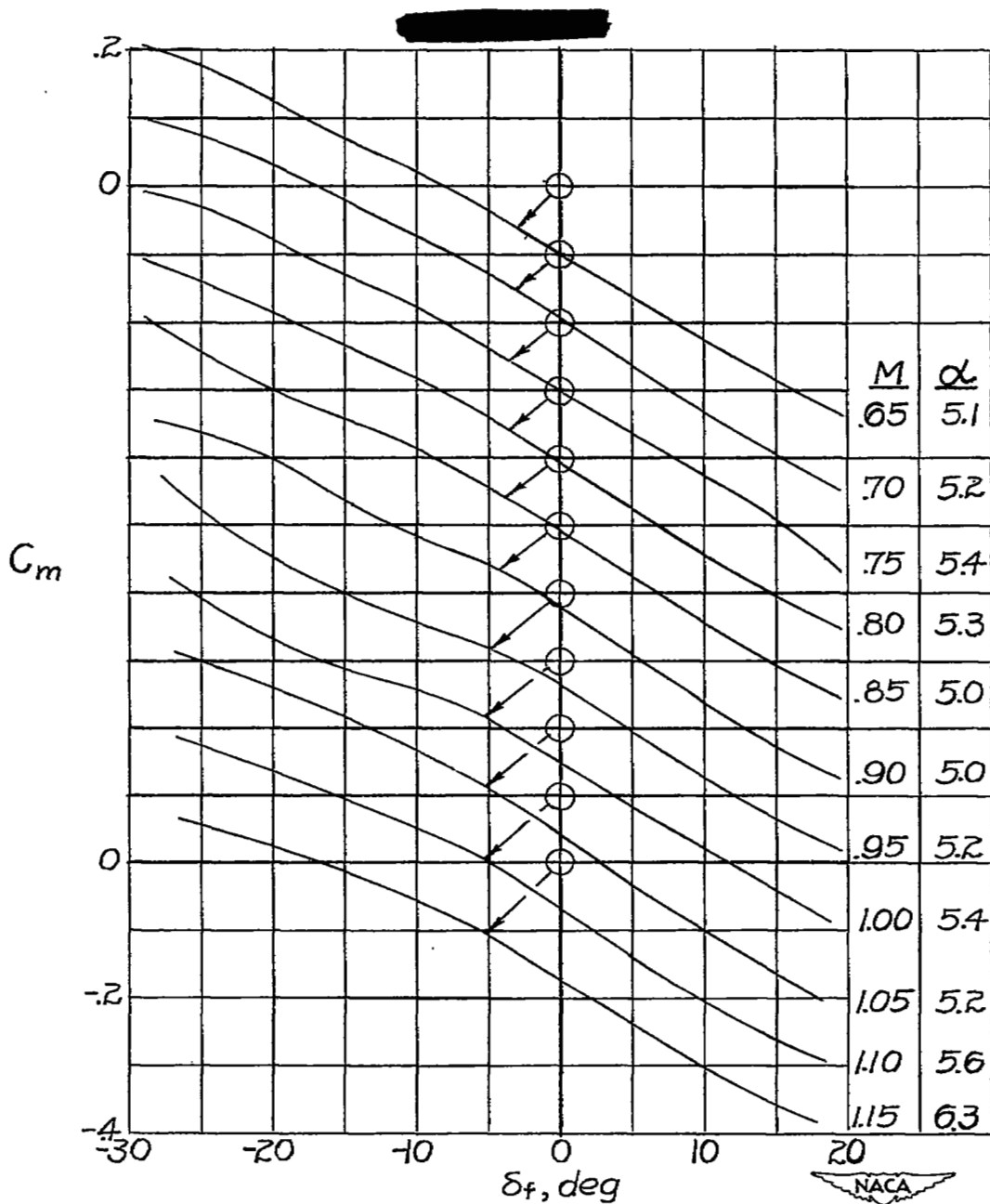
(a) High-dive runs.

Figure 12.- Variation of pitching-moment coefficient with flap deflection throughout Mach number range tested for $\alpha \approx 0^\circ$. NACA 65-009 airfoil; $A = 3.04$; $\Lambda = 35^\circ$; $c_f = 0.25c$; gap unsealed; horn-balanced flap. Moment coefficient given about axis located 18.7 percent mean aerodynamic chord ahead of leading edge of mean aerodynamic chord. Note shift in axis of ordinate scale for different Mach numbers.



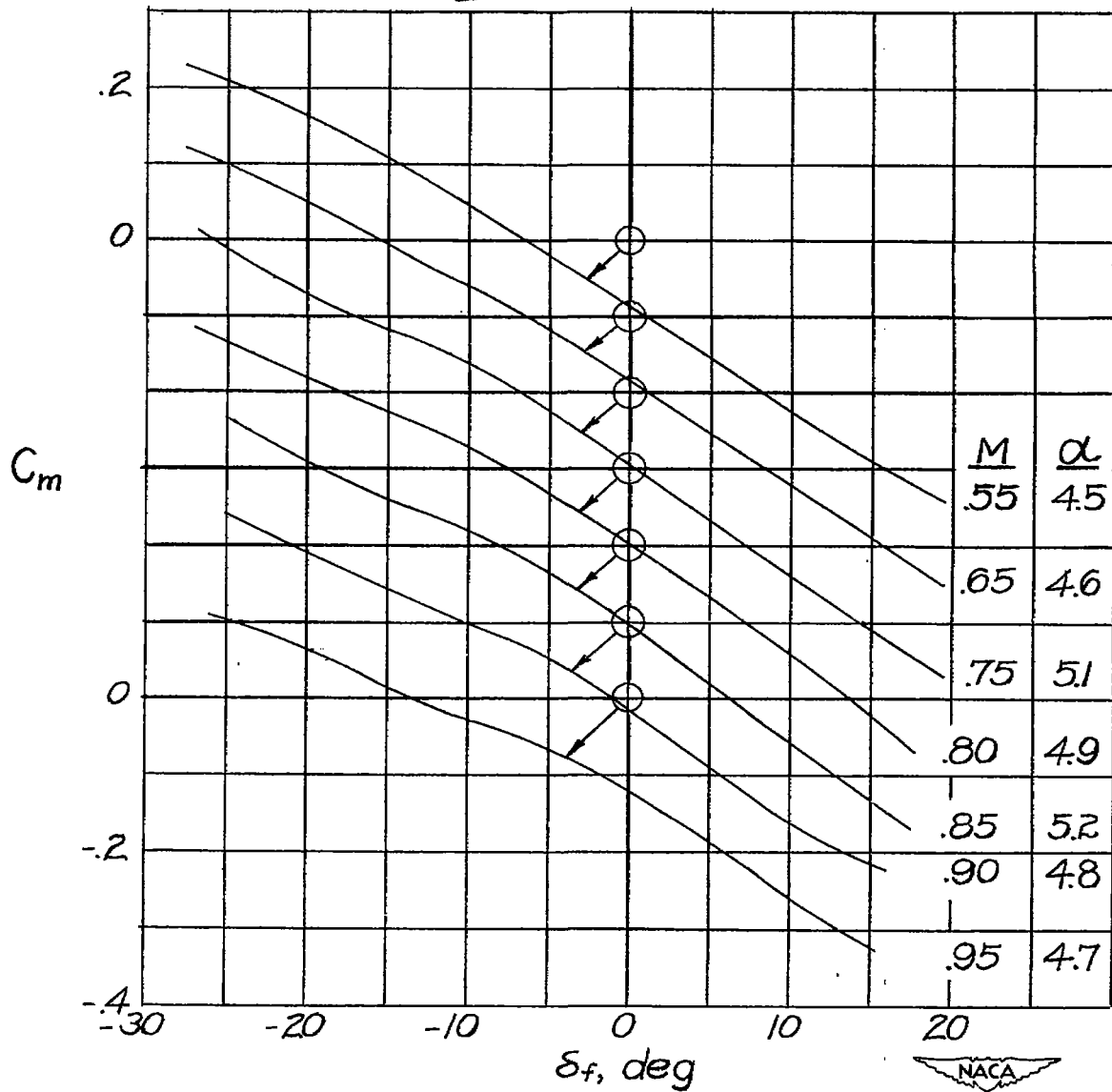
(b) Level-flight runs.

Figure 12.- Concluded.



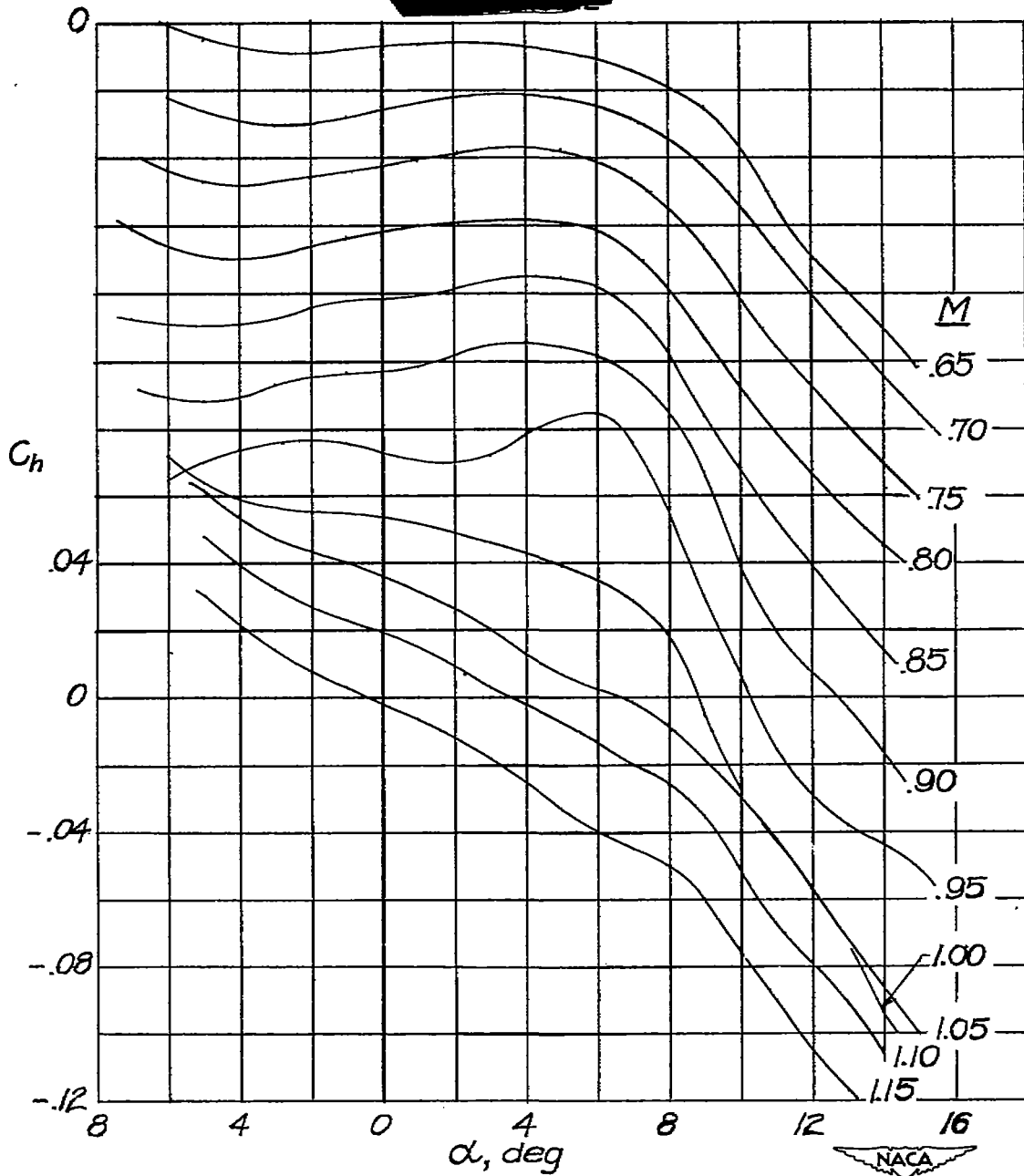
(a) High-dive runs.

Figure 13.— Variation of pitching-moment coefficient with flap deflection throughout Mach number range tested for $\alpha \approx 5^\circ$. NACA 65-009 airfoil; $A = 3.04$; $\Lambda = 35^\circ$; $c_f = 0.25c$; gap unsealed; horn-balanced flap. Moment coefficient given about axis located 18.7 percent mean aerodynamic chord ahead of leading edge of mean aerodynamic chord. Note shift in axis of ordinate scale for different Mach numbers.



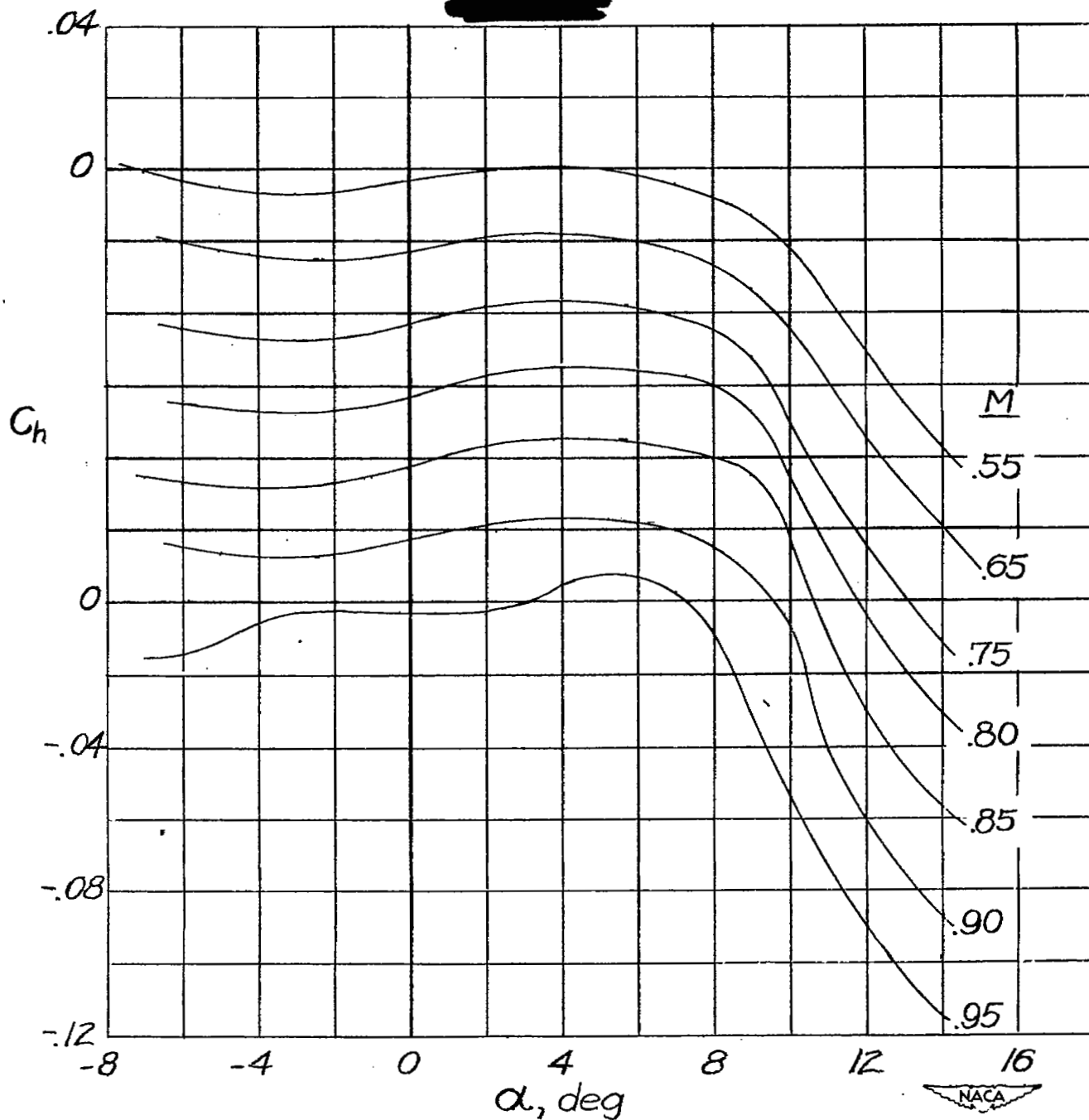
(b) Level-flight runs.

Figure 13.- Concluded.



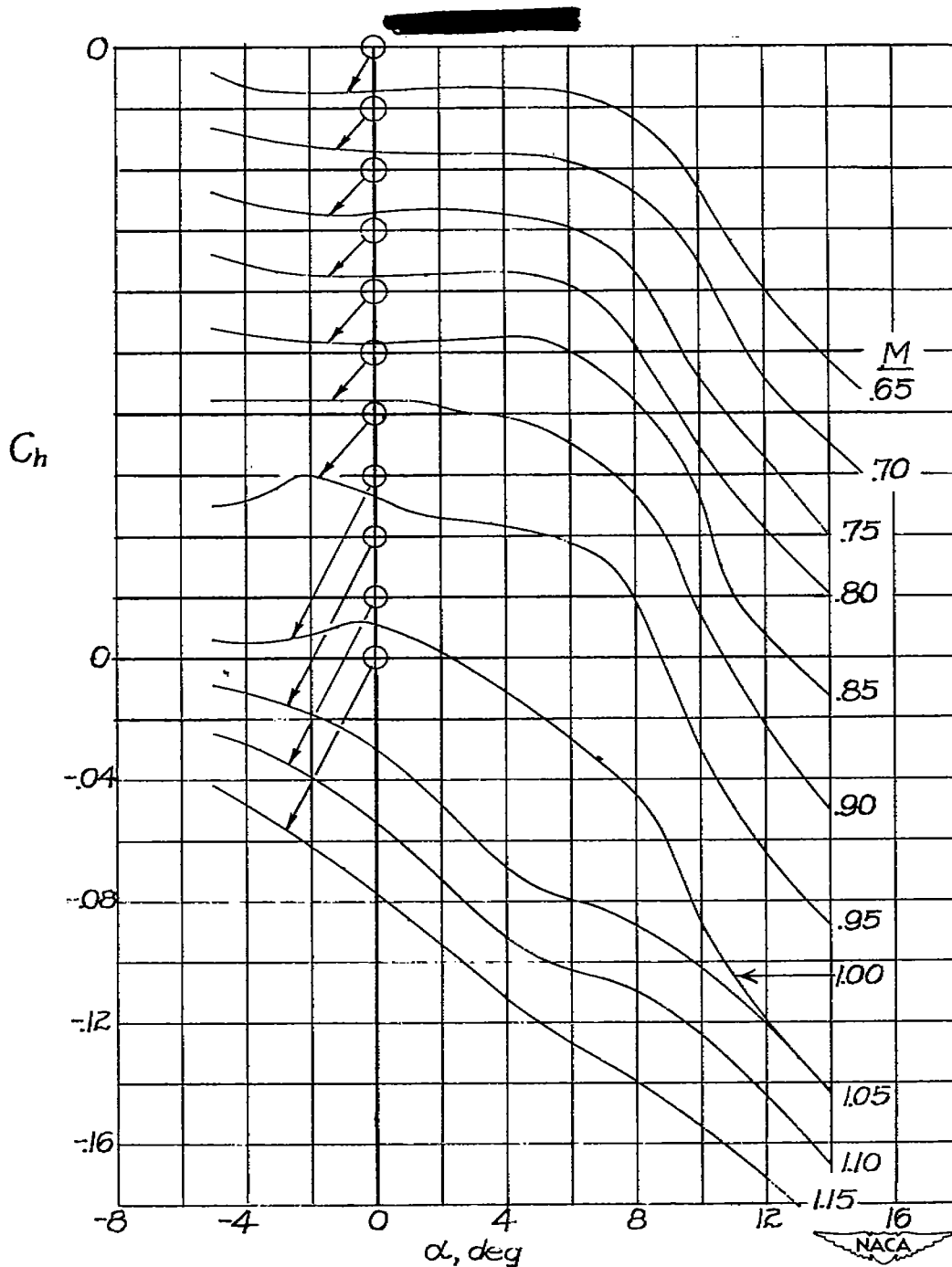
(a) High-dive runs.

Figure 14.- Variation of hinge-moment coefficient with angle of attack throughout Mach number range tested for $\delta_f = 0^\circ$. NACA 65-009 airfoil; $A = 3.04$; $\Lambda = 35^\circ$; $c_f = 0.25c$; gap unsealed; horn-balanced flap. Note shift in axis of ordinate scale for different Mach numbers.



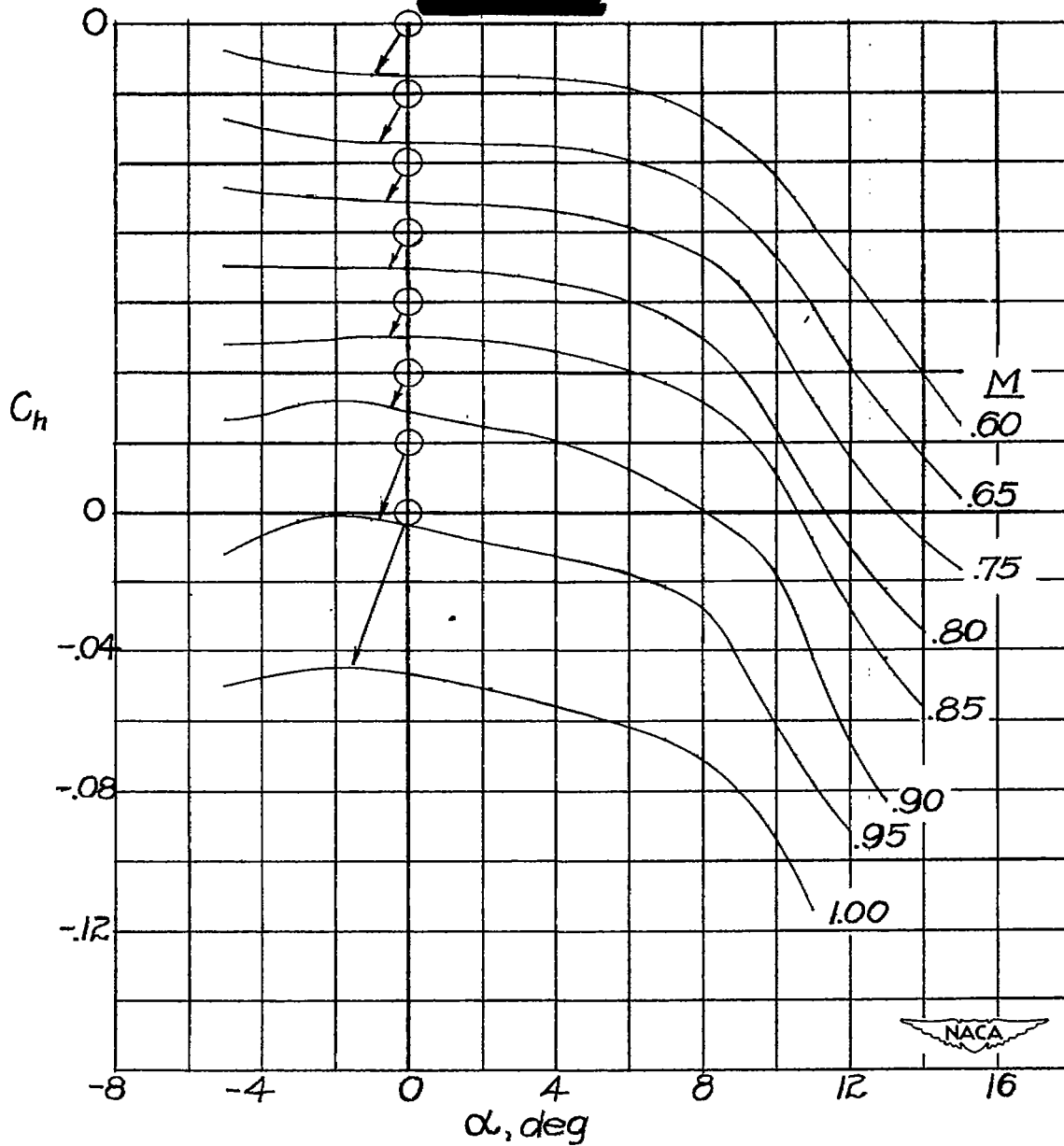
(b) Level-flight runs.

Figure 14.- Concluded.



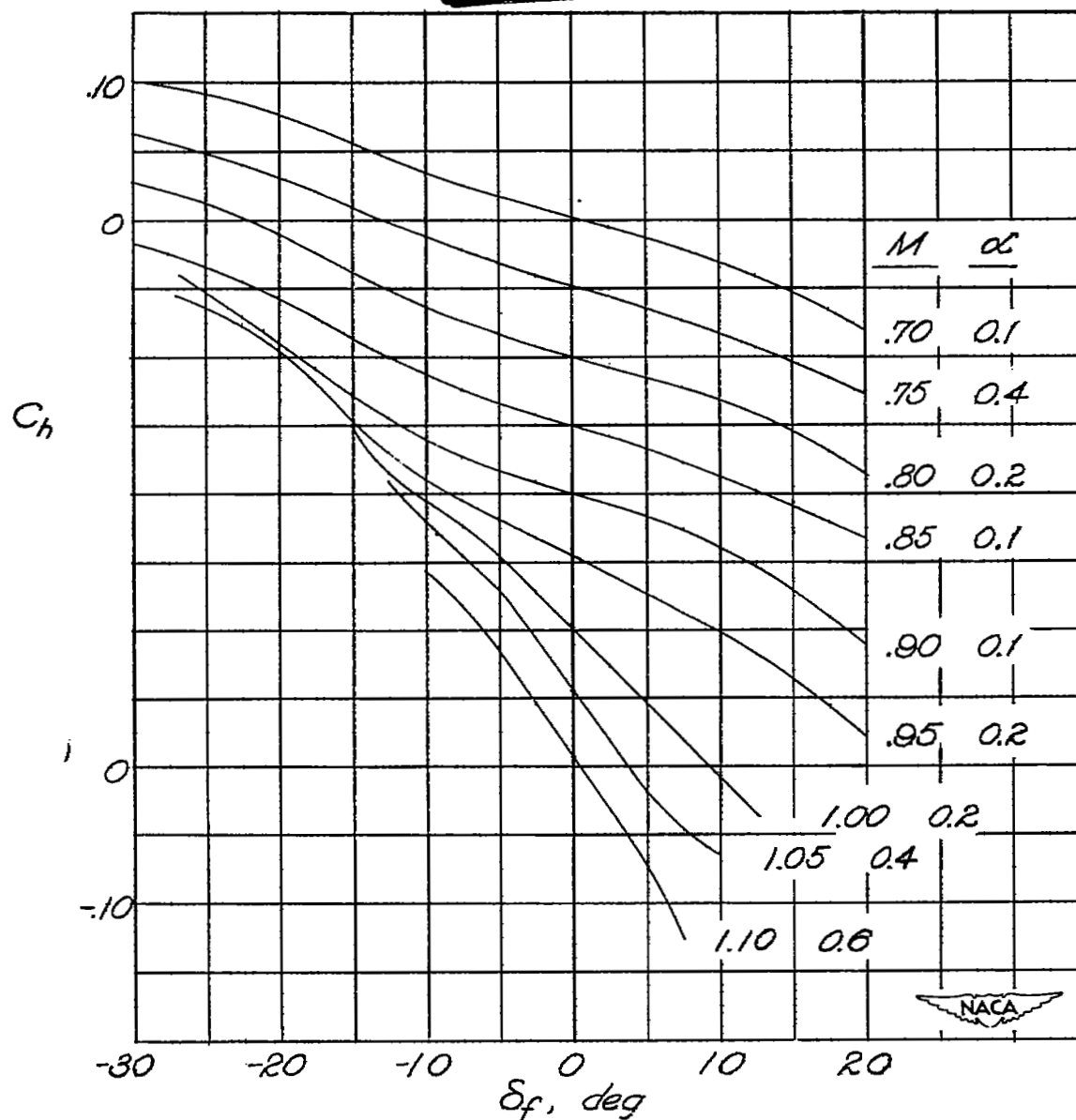
(a) High-dive runs.

Figure 15.— Variation of hinge-moment coefficient with angle of attack throughout Mach number range tested for $\delta_f = 5.0^\circ$. NACA 65-009 airfoil; $A = 3.04$; $\Lambda = 35^\circ$; $c_f = 0.25c$; gap unsealed; horn-balanced flap. Note shift in axis of ordinate scale for different Mach numbers.



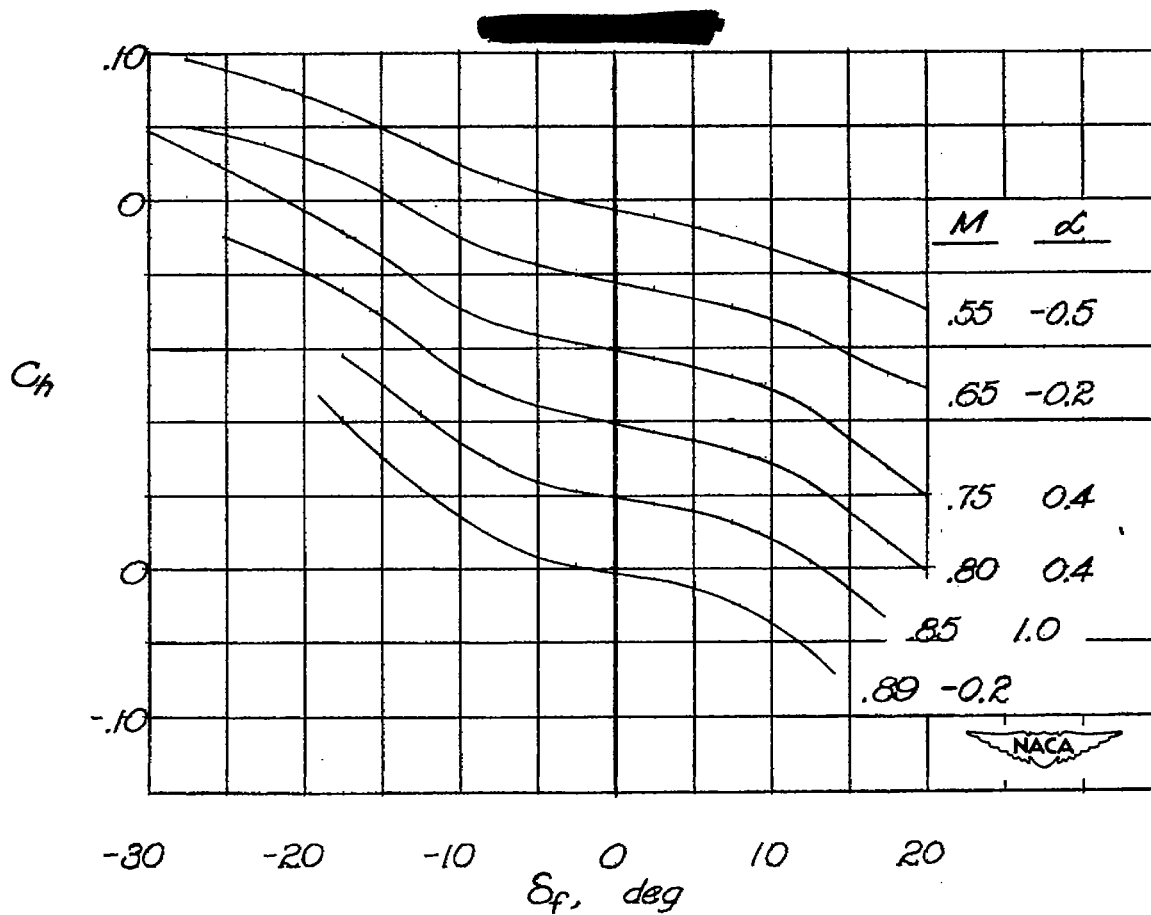
(b) Level-flight runs.

Figure 15.- Concluded.



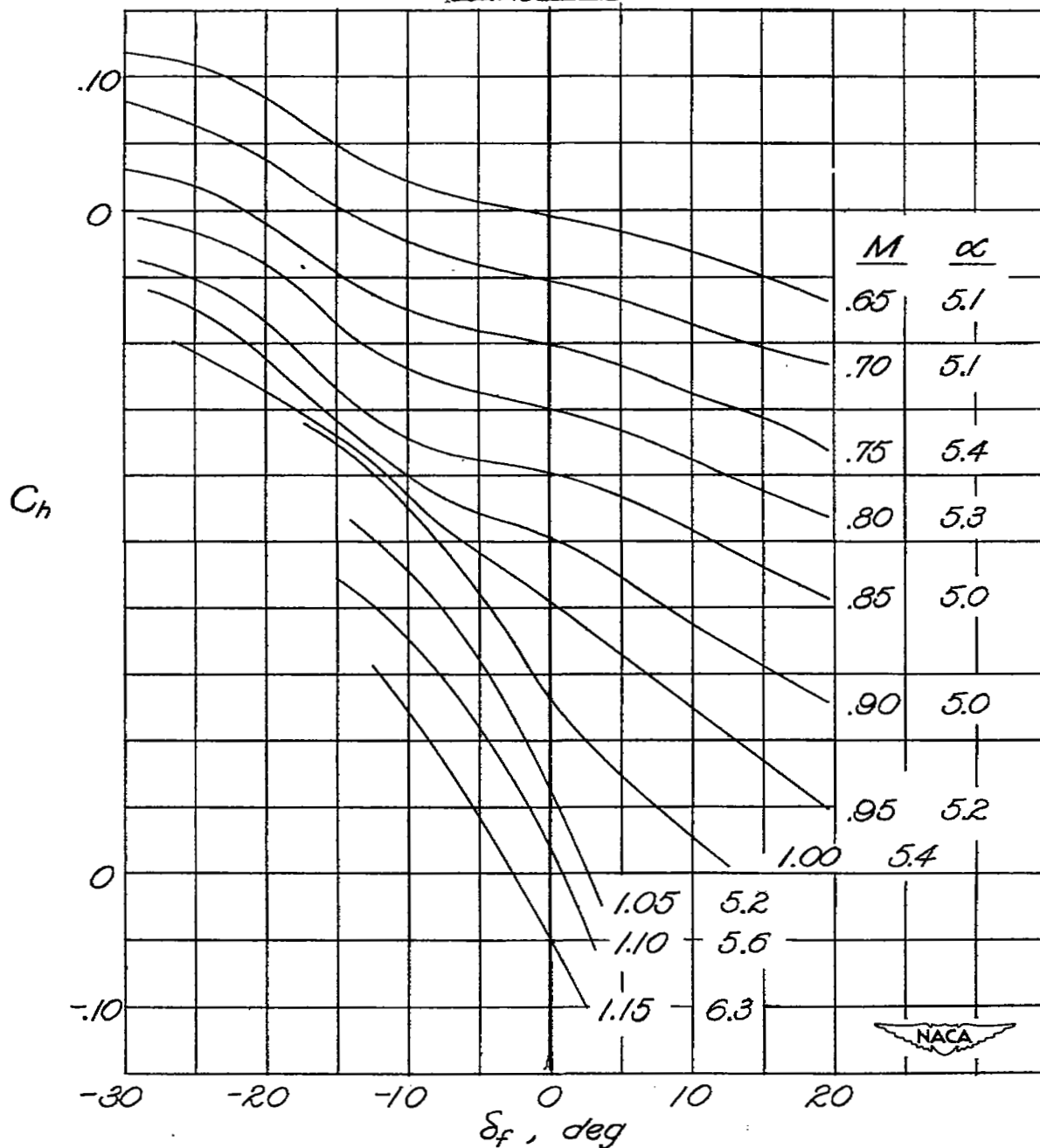
(a) High-dive runs.

Figure 16.— Variation of hinge-moment coefficient with flap deflection throughout Mach number range tested for $\alpha \approx 0^\circ$. NACA 65-009 airfoil; $A = 3.04$; $\Lambda = 35^\circ$; $c_f = 0.25c$; gap unsealed; horn-balanced flap. Note shift in axis of ordinate scale for different Mach numbers.



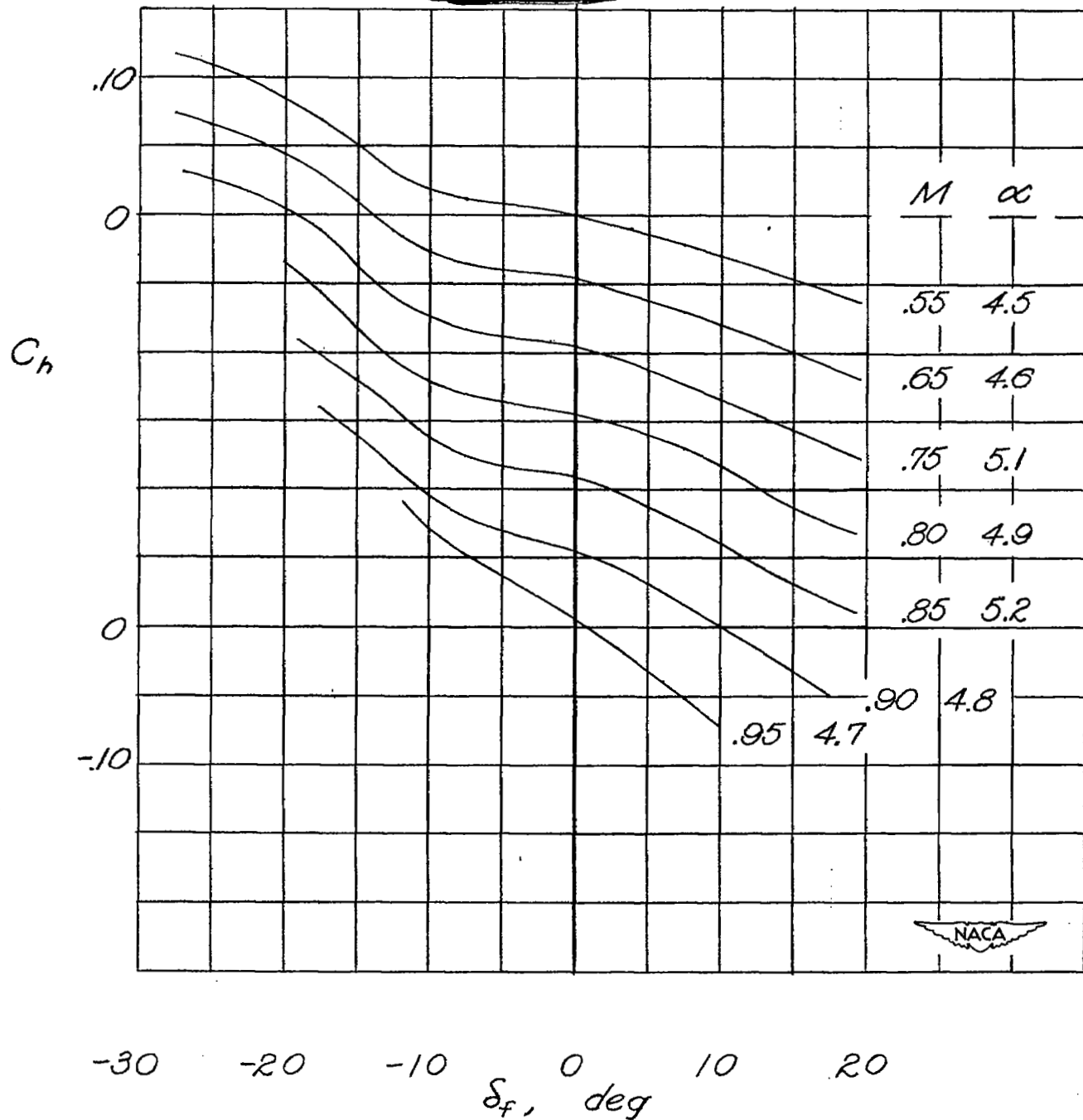
(b) Level-flight runs.

Figure 16.- Concluded.



(a) High-dive runs.

Figure 17.- Variation of hinge-moment coefficient with flap deflection throughout Mach number range tested for $\alpha \approx 5^\circ$. NACA 65-009 airfoil; $\Lambda = 3.04$; $\Lambda = 35^\circ$; $c_f = 0.25c$; gap unsealed; horn-balanced flap. Note shift in axis of ordinate scale for different Mach numbers.



(b) Level-flight runs.

Figure 17.- Concluded.

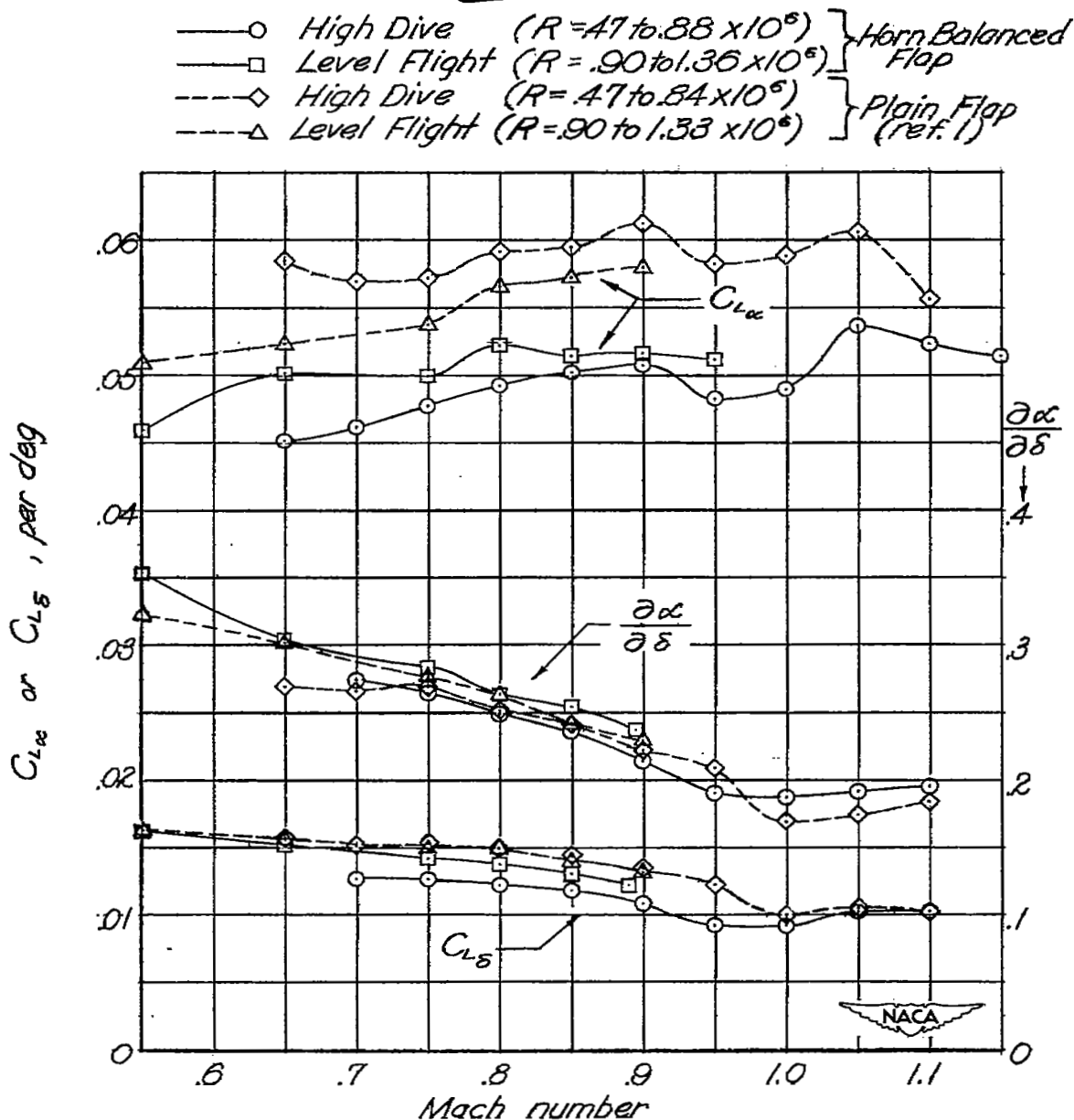
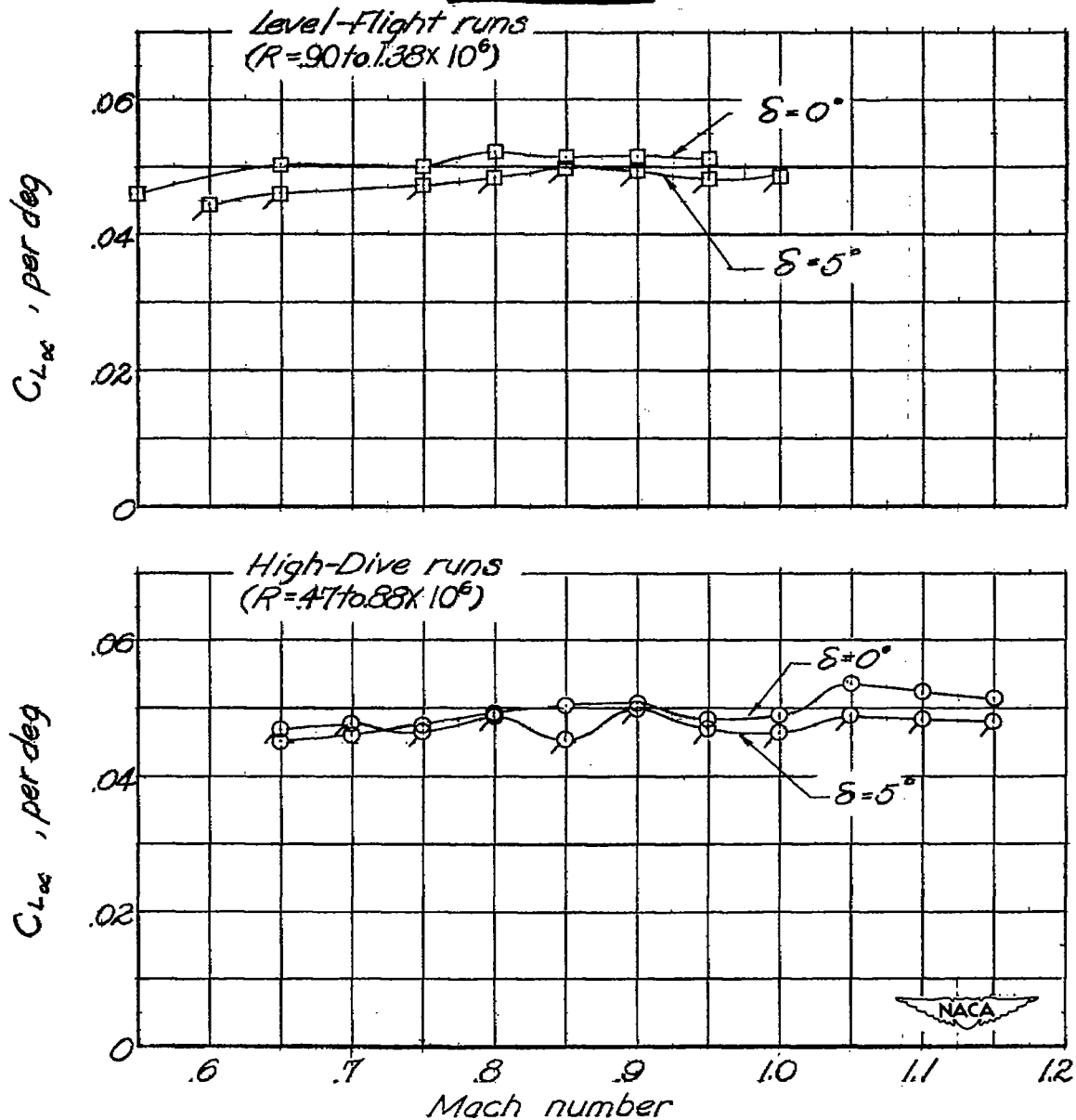
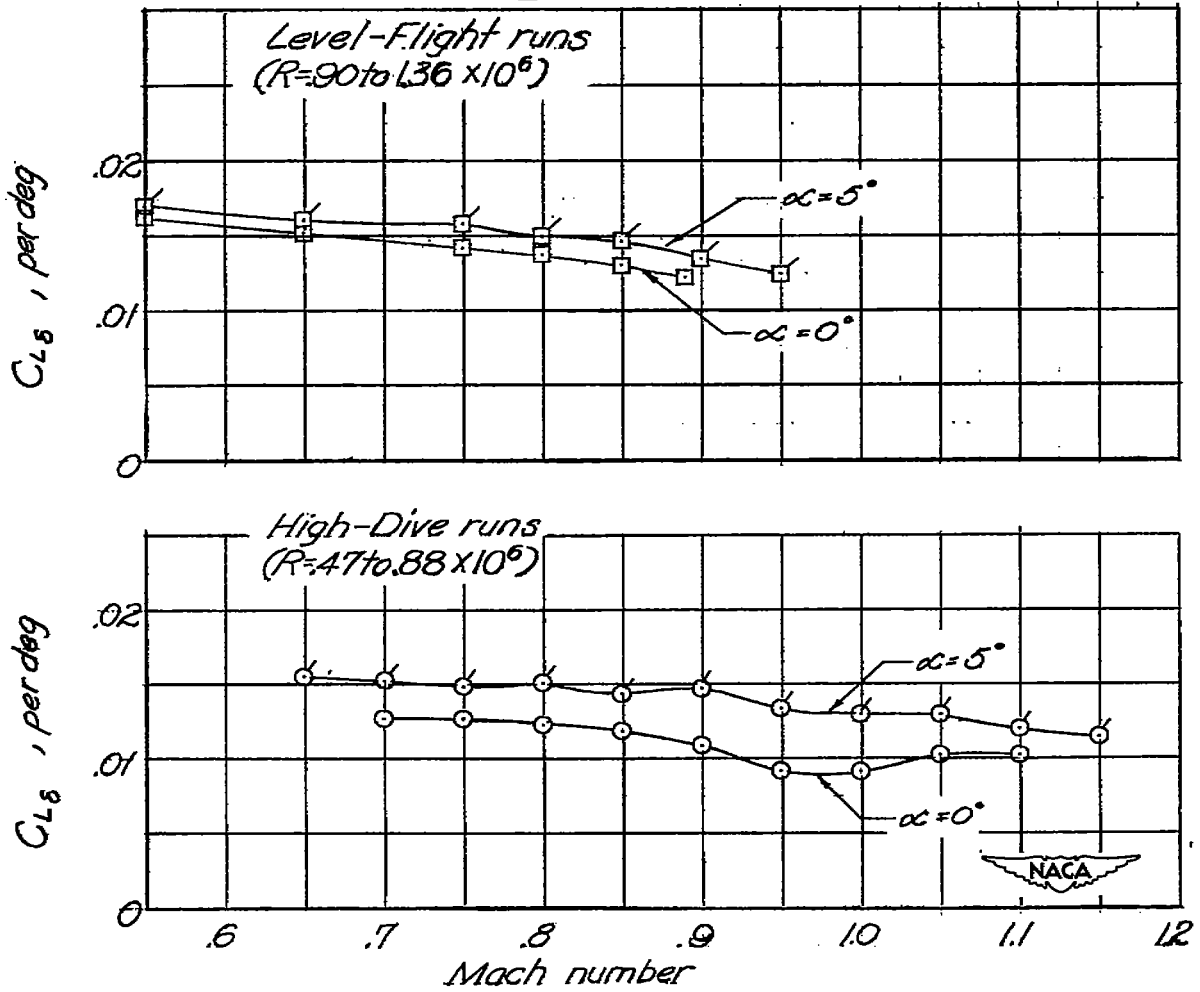


Figure 18.— Variation of airfoil and flap lift effectiveness with Mach number for $\alpha \approx 0^\circ$; $\delta = 0^\circ$. NACA 65-009 airfoil; $A = 3.04$; $\Lambda = 35^\circ$; $c_f = 0.25c$; gap unsealed; horn-balanced flap. Plain-flap data included for comparison.



(a) Effect of flap deflection on lift-curve slope at $\alpha = 0^\circ$.

Figure 19.— Effect of flap deflection and angle of attack on airfoil and flap lift effectiveness. NACA 65-009 airfoil; $A = 3.04$; $\Lambda = 35^\circ$; $c_f = 0.25c$; gap unsealed; horn-balanced flap.



(b) Effect of angle of attack on flap effectiveness at $\delta_f = 0^\circ$.

Figure 19.- Concluded.

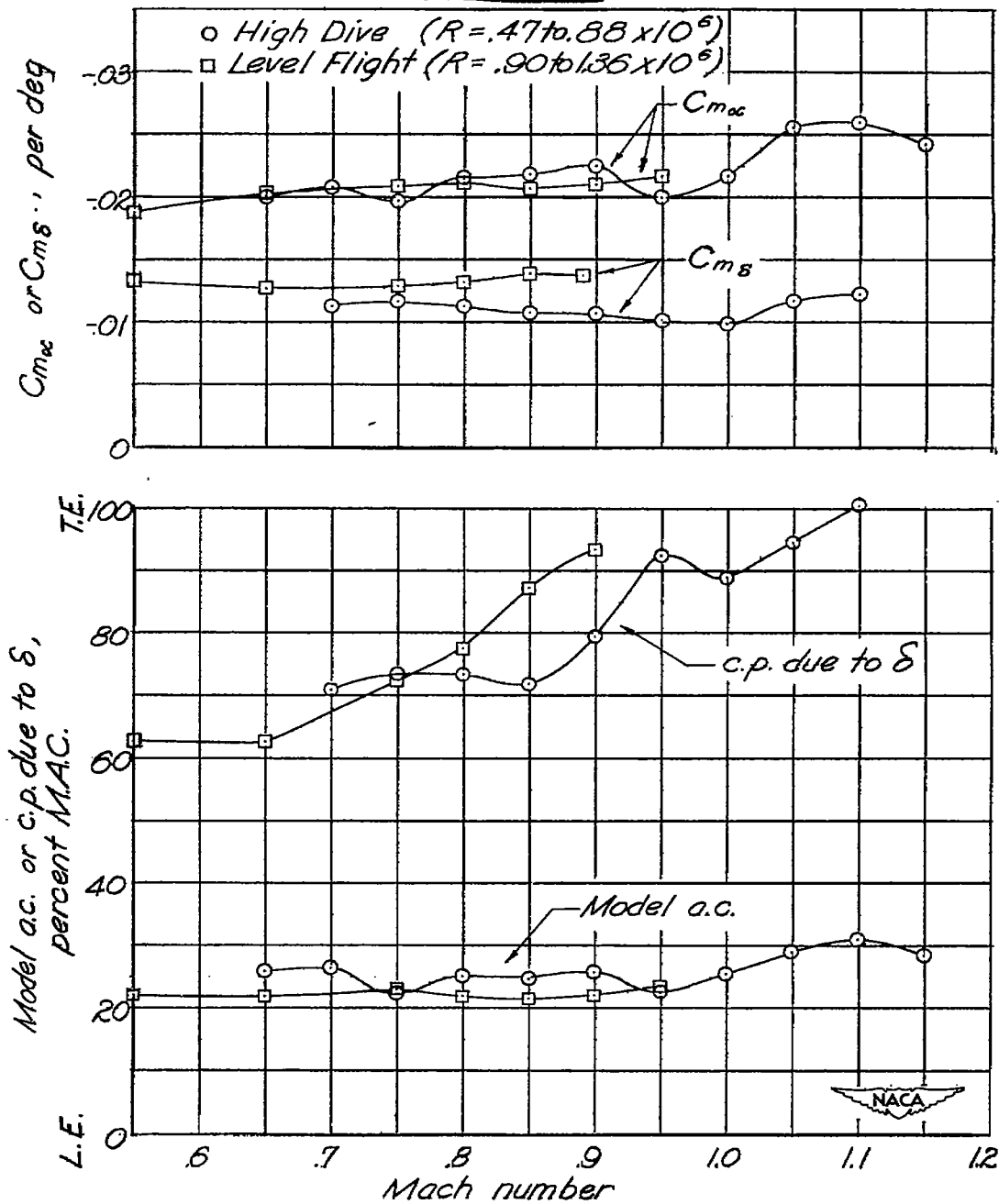


Figure 20.— Variation of airfoil and flap pitching-moment characteristics with Mach number for $\alpha \approx 0^\circ$; $\delta_f = 0^\circ$. NACA 65-009 airfoil; $A = 3.04$; $\Lambda = 35^\circ$; $c_f = 0.25c$; gap unsealed; horn-balanced flap. Pitching moments measured about axis located 18.7 percent mean aerodynamic chord forward of leading edge of mean aerodynamic chord.

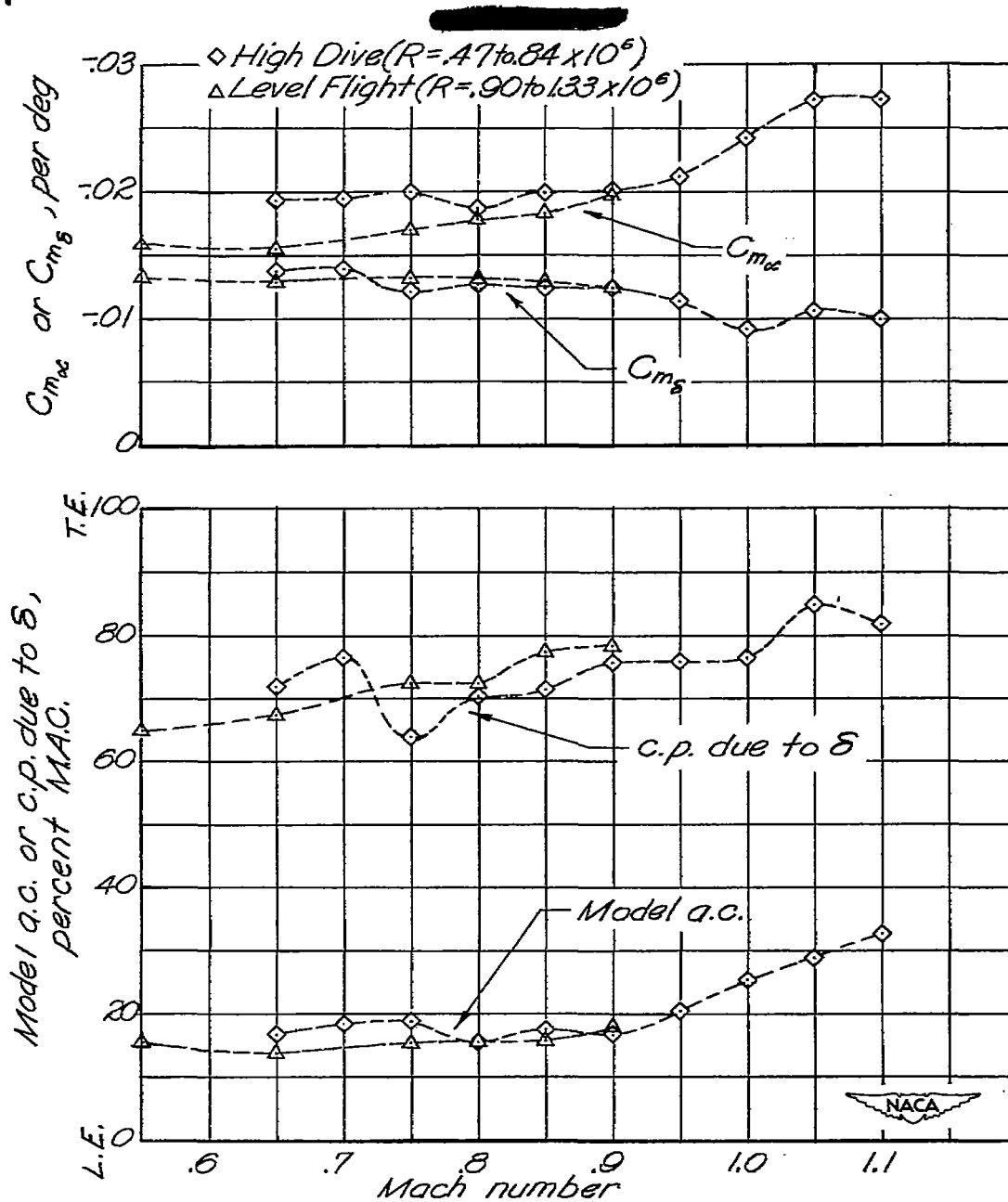
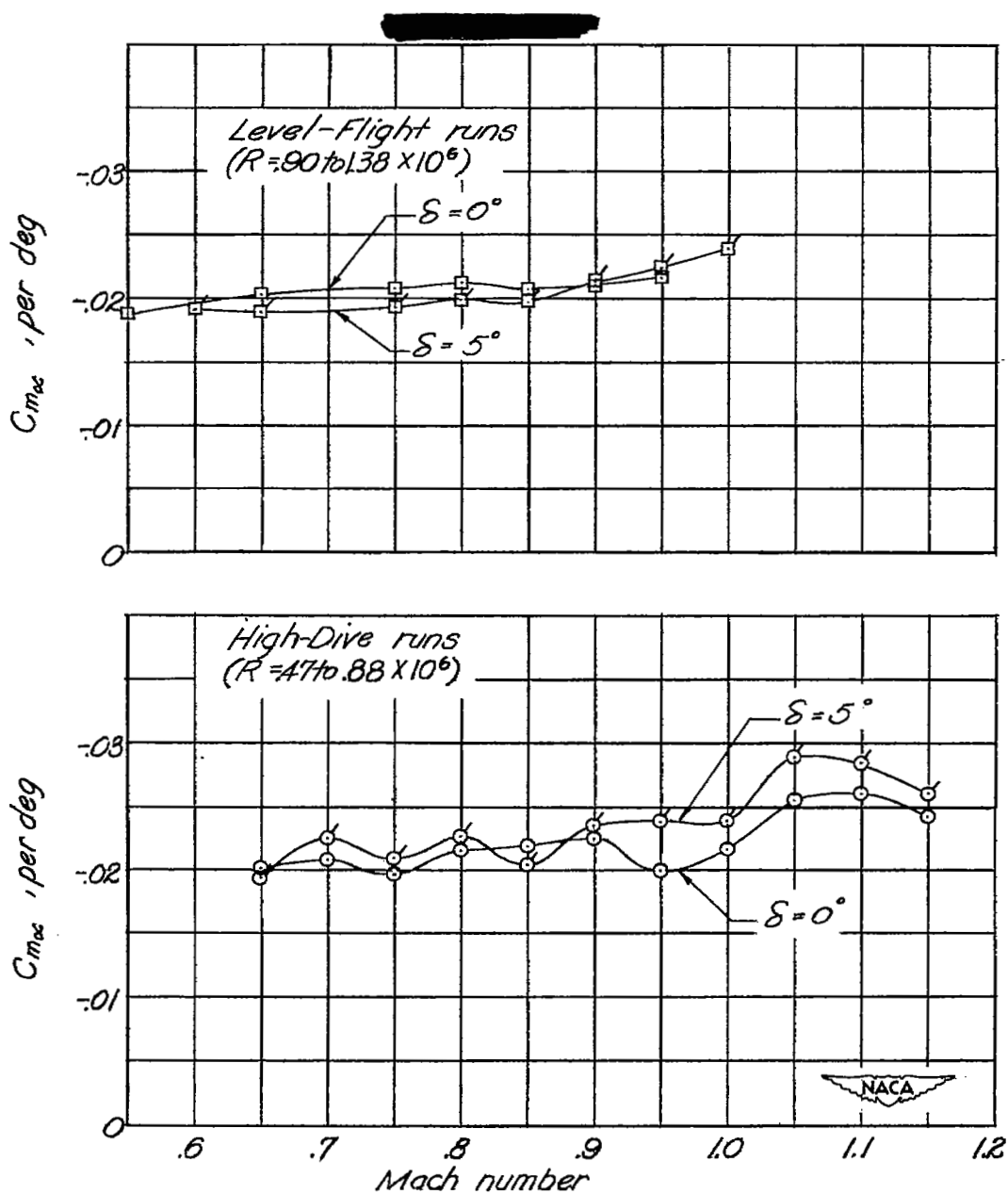
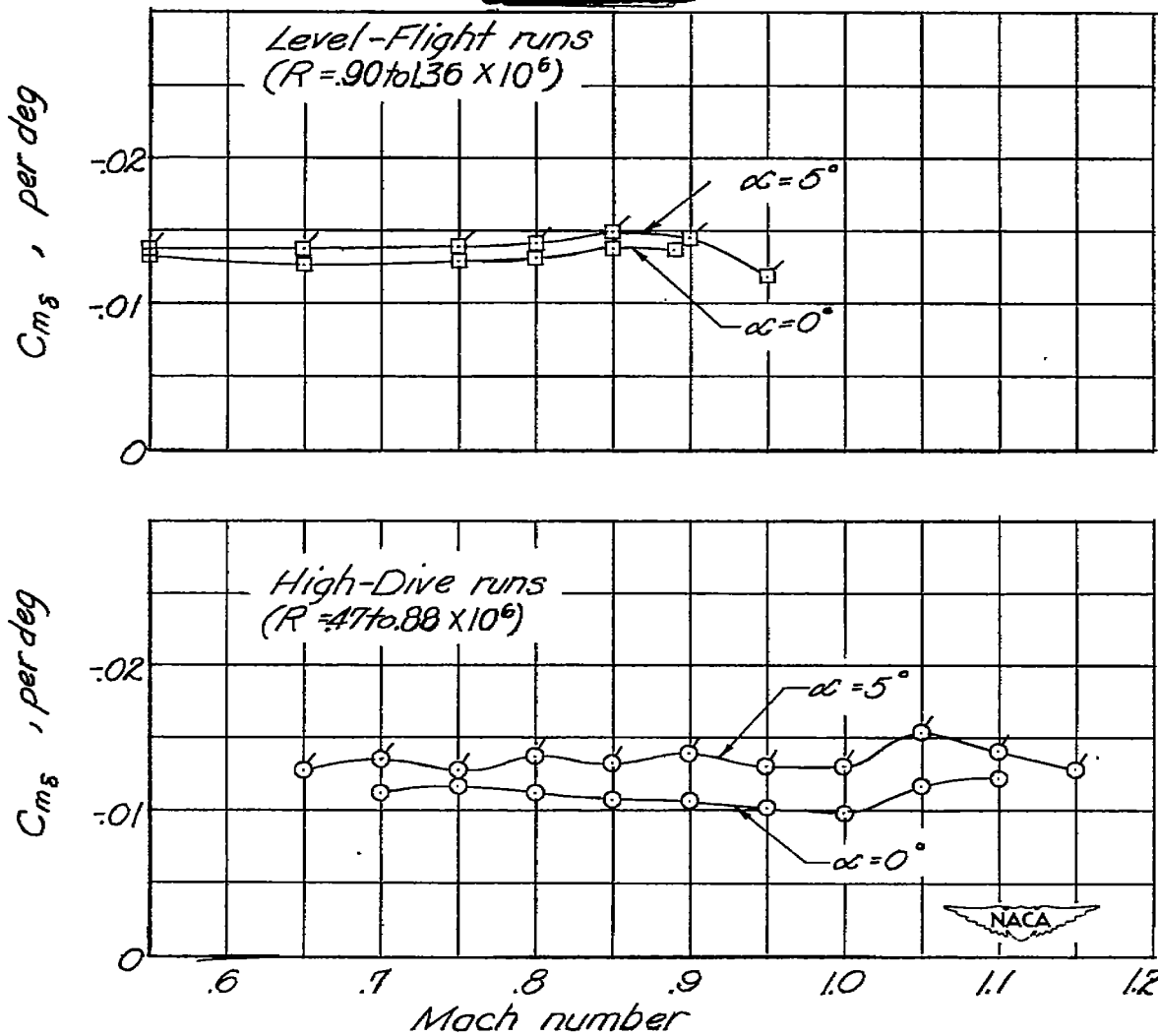


Figure 21.— Variation of airfoil and flap pitching-moment characteristics with Mach number for $\alpha \approx 0^\circ$; $\delta_f = 0^\circ$. NACA 65-009 airfoil; $A = 3.04$; $\Lambda = 35^\circ$; $c_f = 0.25c$; gap unsealed; plain flap. Pitching moments measured about axis located 16 percent mean aerodynamic chord forward of leading edge of mean aerodynamic chord.



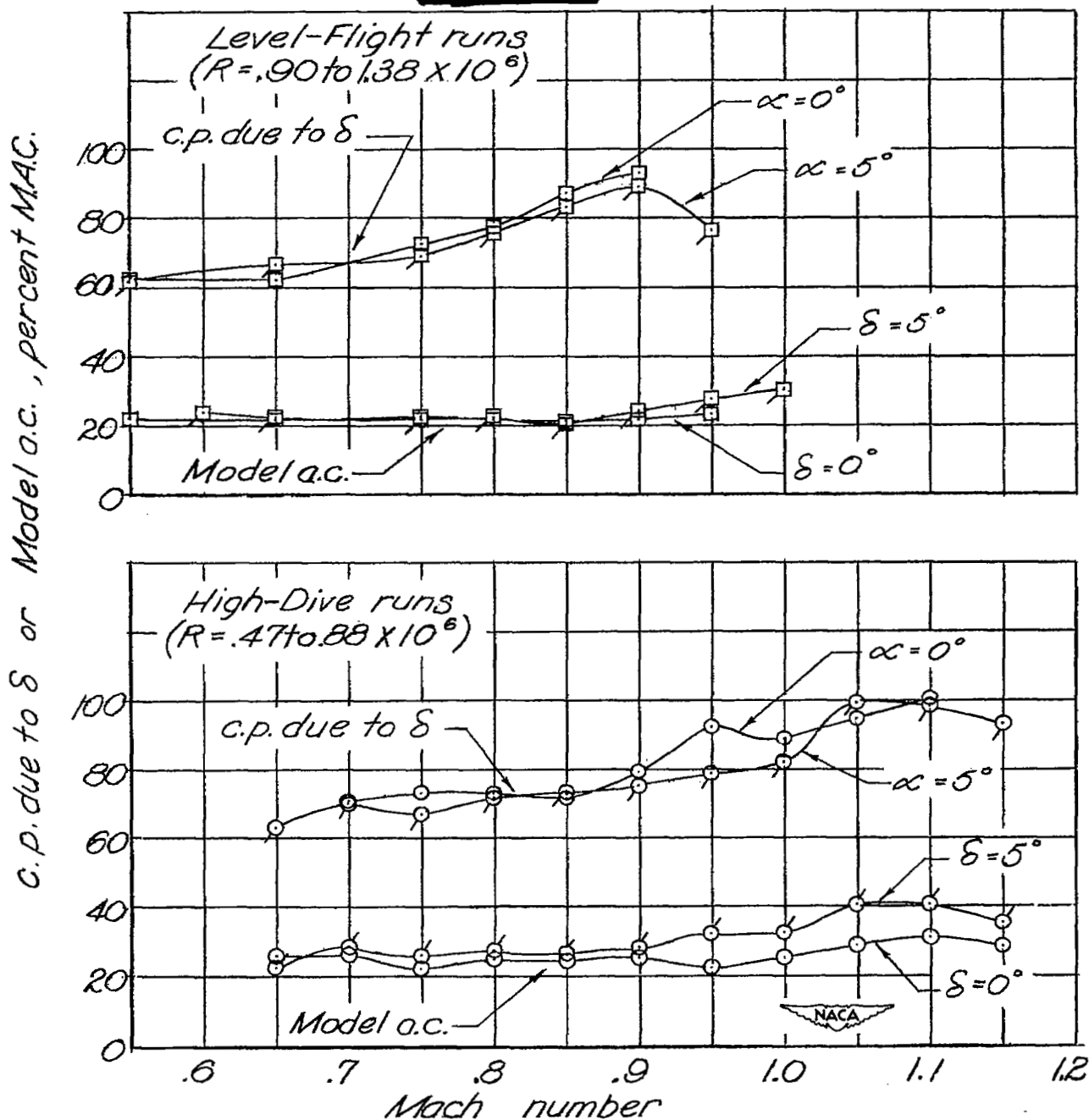
(a) Effect of flap deflection on airfoil pitching moments at $\alpha = 0^\circ$.

Figure 22.— Effect of flap deflection and angle of attack on airfoil and flap pitching-moment characteristics. NACA 65-009 airfoil; $A = 3.04$; $\Lambda = 35^\circ$; $c_f = 0.25c$; gap unsealed; horn-balanced flap. Pitching moments measured about axis located 18.7 percent mean aerodynamic chord forward of leading edge of mean aerodynamic chord.



(b) Effect of angle of attack on flap pitching moments at $\delta_p = 0^\circ$.

Figure 22.- Continued.



(c) Effect of angle of attack on center of pressure due to flap deflection and effect of flap deflection on aerodynamic-center location.

Figure 22.— Concluded.

- ~~SECRET~~
- High Dive } Horn-Balanced Flap
 - Level Flight } Horn-Balanced Flap
 - ◇--- High Dive } Plain Flap (ref. 1)
 - △--- Level Flight } Plain Flap (ref. 1)

	Mach number	Reynolds number
High Dive	.65	$.47 \times 10^6$
"	1.15	$.88 \times 10^6$
Level Flight	.55	$.90 \times 10^6$
"	.90	1.33×10^6

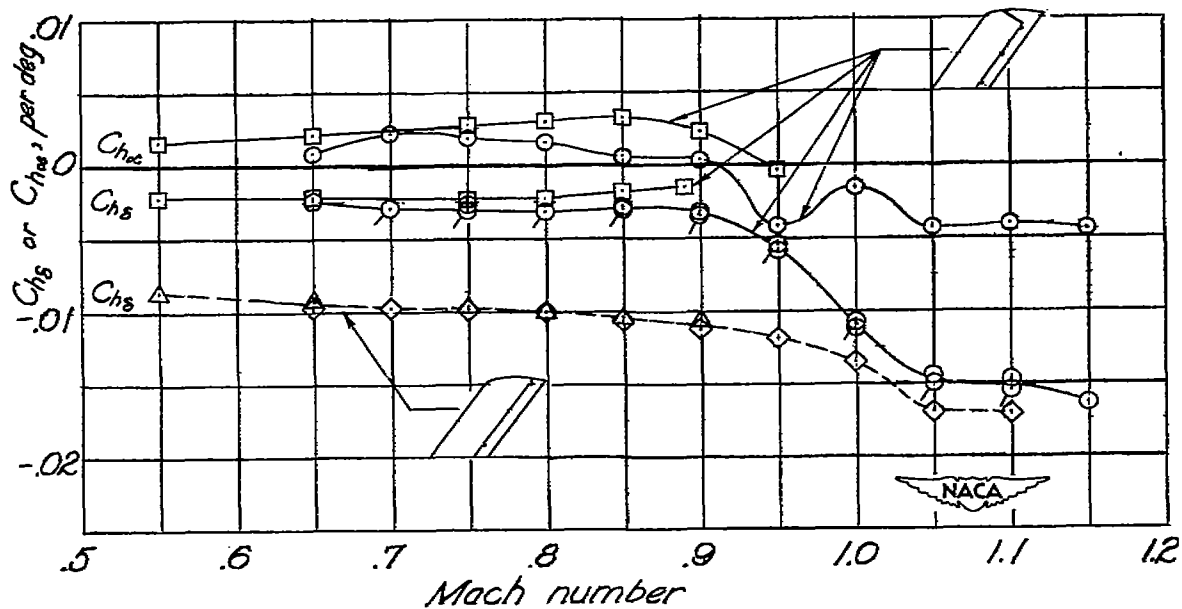
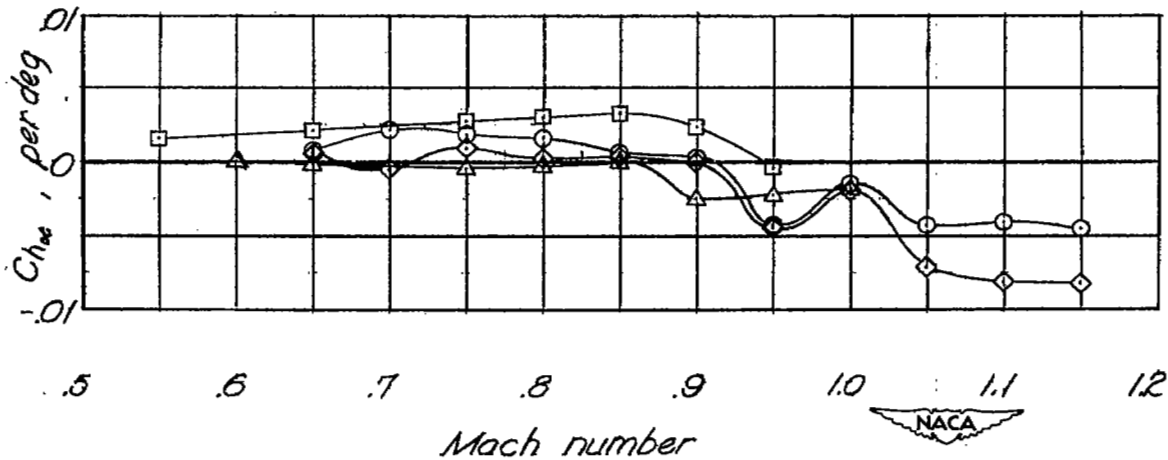


Figure 23.— Variation with Mach number of rate of change of hinge-moment coefficient with change in flap deflection and with change in angle of attack measured at $\alpha \approx 0^\circ$, $\delta_f = 0^\circ$. NACA 65-009 airfoil; $A = 3.04$; $\Lambda = 35^\circ$; $c_f = 0.25c$; gap unsealed; horn-balanced flap. Plain-flap data from reference 1 included for comparison.

~~SECRET~~

- High Dive } $\delta = 0^\circ$
 □ Level Flight }
 ◇ High Dive } $\delta = 5^\circ$
 △ Level Flight }

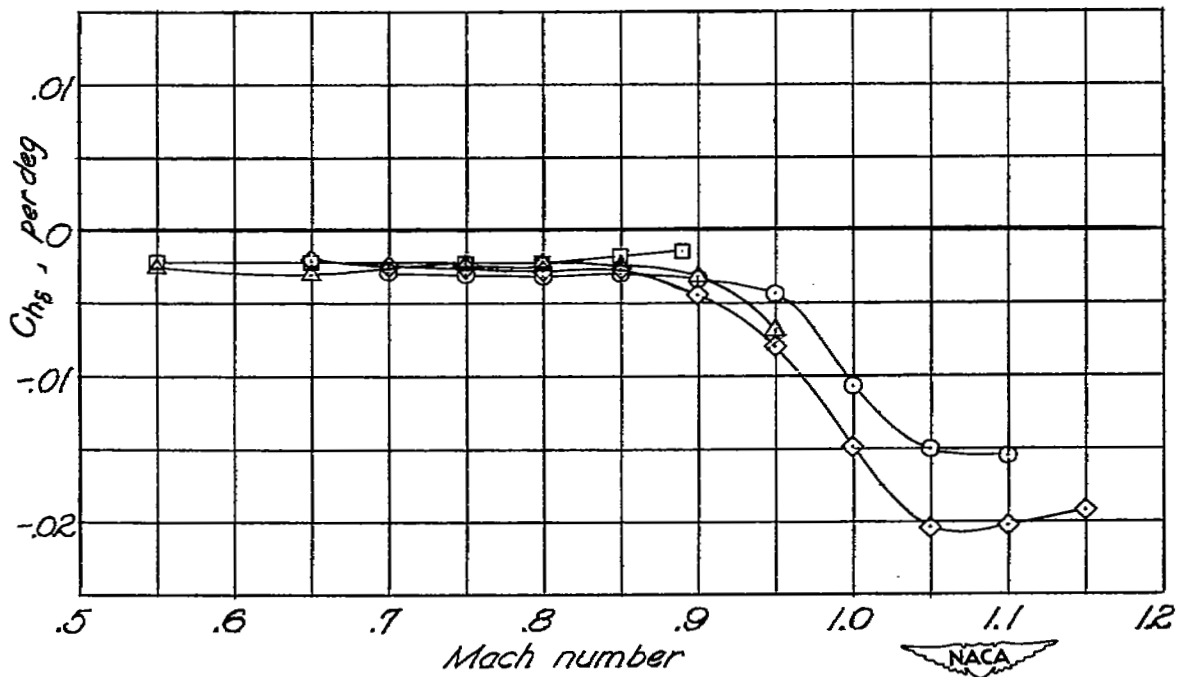


(a) Effect of flap deflection on rate of change of hinge-moment coefficient with angle of attack measured at $\alpha = 0^\circ$.

Figure 24.— Effect of flap deflection and angle of attack on hinge moment due to angle of attack and flap deflection, respectively.

NACA 65-009 airfoil; $A = 3.04$; $\Lambda = 35^\circ$; $c_f = 0.25c$; gap unsealed; horn-balanced flap.

- High Dive } $\alpha \approx 0^\circ$
 □ Level Flight }
 ◇ High Dive } $\alpha \approx 5^\circ$
 △ Level Flight }



(b) Effect of angle of attack on rate of change of hinge-moment coefficient with flap deflection measured at $\delta_f = 0^\circ$.

Figure 24.- Concluded.

NASA Technical Library



3 1176 01436 7206